**Cláudia Catarina da Costa Ralo**

Licenciatura em Ciências da Engenharia Química e Bioquímica

# Coupling Organic Substrate Removal to Methane Production in a Fully Biological Microbial Electrolysis Cell

Dissertação para obtenção do Grau de Mestre em Engenharia Química e Bioquímica

Orientador: Mauro Majone, Professor Associado, Sapienza Univeristy of Rome
Co-orientador: Marianna Villano, Doutora, Sapienza University of Rome

Júri:

Presidente: Prof. Doutora Isabel Maria Rola Coelhoso
Arguente: Doutor Svetlozar Gueorguiev Velizarov
Vogais: Prof. Doutora Maria Ascensão Carvalho Fernandes Miranda Reis
Prof. Doutor Mauro Majone

FACULDADE DE CIÊNCIAS E TECNOLOGIA
UNIVERSIDADE NOVA DE LISBOA

**Março 2013**

**Cláudia Catarina da Costa Ralo**

Licenciatura em Ciências da Engenharia Química e Bioquímica

# Coupling Organic Substrate Removal to Methane Production in a Fully Biological Microbial Electrolysis Cell

Dissertação para obtenção do Grau de Mestre em Engenharia Química e Bioquímica

Orientador: Mauro Majone, Professor Associado, Sapienza Univeristy of Rome
Co-orientador: Marianna Villano, Doutora, Sapienza University of Rome

Júri:

Presidente: Prof. Doutora Isabel Maria Rola Coelhoso
Arguente: Doutor Svetlozar Gueorguiev Velizarov
Vogais: Prof. Doutora Maria Ascensão Carvalho Fernandes Miranda Reis
Prof. Doutor Mauro Majone

**Março 2013**

*For my family*

## Aknowledgments

The accomplishment of this thesis would not be possible without the contributions of some individuals, to whom I would like to thank.

I would like to express my deep gratitude to Professor Mauro Majone and Professor Maria Ascensão Reis for the opportunity to have this experience abroad.

I would like to demonstrate my sincere appreciation to Doctor Marianna Villano and Professor Mauro Majone, my supervisors, for the invaluable support, scientific guidance, and for always have shared their knowledge and gave me the best advices. To Roberta Verdini and Stefano Scardala for all the patience and attention. To all the members of Lab 026 for kindly integrated me.

To Professor Mario Beccari, Professor Daniela Ferro and Professor Joaquim Vital, for the help and advices on specific parts of this work.

To my family, for their understanding, endless patience and encouragement when it was most required! A special thank you to my brother João.

To my friends for always being there. And a very special thank you to my university friends, for the inspiration and strength!

## Resumo

As células de electrólise microbiana (CEMs) são uma técnica inovadora e emergente fundamentada na utilização de eléctrodos de estado sólido, que estimulam o metabolismo microbiano para o tratamento de efluentes e produção paralela de produtos de valor acrescentado (como o metano).

Neste trabalho estudou-se o desempenho de uma CEM composta por duas câmaras, onde no ânodo ocorria a oxidação da matéria orgânica e no cátodo a produção de metano. O inóculo do ânodo era composto por lamas activadas, enquanto o do cátodo consistia em lamas anaeróbicas que continham microorganismos metanogénicos. Durante a operação, o bioânodo foi alimentado continuamente, com soluções sintéticas em meio anaeróbico basal sendo a carga orgânica de cerca de 1 g $L^{-1}$ $d^{-1}$, referente à Carência Química de Oxigénio (CQO). No início (ensaio I), o alimento consistia principalmente em acetato sendo posteriormente substituído por uma mistura mais complexa (ensaio II), que continha outros compostos orgânicos solúveis para além deste. Para ambas as condições, o potencial do ânodo foi controlado a -0.1 V *vs.* eléctrodo padrão de hidrogénio, através de um potencióstato. Durante o ensaio I, mais de 80% do acetato fornecido ao sistema foi anaerobicamente oxidado no ânodo, e a corrente eléctrica resultante foi recuperada como metano no cátodo (obtendo uma eficiência de captura catódica (ECC) de cerca de 115%). Nestas condições obteve-se cerca de 170 % de eficiência energética média do sistema (i.e., a energia recuperada como metano relativamente à energia fornecida). No entanto, o desempenho do reactor diminuiu no decorrer deste ensaio. Ao longo do ensaio II, observou-se uma oxidação de substrato acima dos 60% (referente à CQO). A corrente eléctrica produzida (com uma eficiência coulombica de 57%) foi também recuperada como metano, sendo a ECC de 90%. Neste ensaio, a eficiência energética da CEM foi aproximadamente 170%. Durante toda a experiência, observou-se um crescimento de biomassa muito reduzido no ânodo, por sua vez o ião amónio foi transferido através da membrana catiónica e concentrou-se no cátodo. Com o objectivo de obter uma visão mais aprofundada do desempenho do reactor, realizaram-se provas com marcador e análises de microscopia electrónica de varrimento.

Em conclusão, este estudo sugere o enorme potencial da CEM no tratamento de águas residuais de baixa carga orgânica, aliando uma elevada eficiência energética à baixa produção de lamas.



***Termos-chave:*** *Célula de Electrólise Microbiana, tratamento de águas residuais, oxidação de matéria orgânica, produção de metano, eficiência energética.*

## Abstract

Microbial electrolysis cells (MECs) are an innovative and emerging technique based on the use of solid-state electrodes to stimulate microbial metabolism for wastewater treatment and simultaneous production of value-added compounds (such as methane).

This research studied the performance of a two-chamber MEC in terms of organic matter oxidation (at the anode) and methane production (at the cathode). MEC's anode had been previously inoculated with an activated sludge, whereas the cathode chamber inoculum was an anaerobic sludge (containing methanogenic microorganisms). During the experimentation, the bioanode was continuously fed with synthetic solutions in anaerobic basal medium, at an organic load rate (OLR) of around 1 g $L^{-1}$ $d^{-1}$, referred to the chemical oxygen demand (COD). At the beginning (Run I), the feeding solution contained acetate and subsequently (Run II) it was replaced with a more complex solution containing soluble organic compounds other than acetate. For both conditions, the anode potential was controlled at -0.1 V *vs.* standard hydrogen electrode, by means of a potentiostat. During Run I, over 80% of the influent acetate was anaerobically oxidized at the anode, and the resulting electric current was recovered as methane at the cathode (with a cathode capture efficiency, CCE, accounting around 115 %). The average energy efficiency of the system (i.e., the energy captured into methane relative to the electrical energy input) under these conditions was over 170%. However, reactor's performance decreased over time during this run. Throughout Run II, a substrate oxidation over 60% (on COD basis) was observed. The electric current produced (57% of coulombic efficiency) was also recovered as methane, with a CCE of 90%. For this run the MEC's average energy efficiency accounted for almost 170 %. During all the experimentation, a very low biomass growth was observed at the anode whereas ammonium was transferred through the cationic membrane and concentrated at the cathode. Tracer experiments and scanning electron microscopy analyses were also carried out to gain a deeper insight into the reactor performance and also to investigate the possible reasons for partial loss of performance.

In conclusion, this research suggests the great potential of MEC to successfully treat low-strength wastewaters, with high energy efficiency and very low sludge production.

**Keywords:** *Microbial electrolysis cell, wastewater treatment, organic matter oxidation, methane production, energy efficiency*.

## Table of Contents


1. Literature Review 1
   1.1. Bioelectrochemical Systems 2
      1.1.1. Microbial Fuel Cell – electricity generation 3
      1.1.2. Microbial Electrolysis Cell – hydrogen generation 6
   1.2. Coupling organic substrate removal to methane production 8
2. Research objectives 13
3. Materials and methods 15
   3.1. Microbial electrolysis cell design and setup 15
   3.2. Microbial electrolysis cell operation 17
   3.3. Tracer experiment 19
   3.4. Control and data acquisition 24
      3.4.1. Potentiostatic system 24
   3.5. Analytical measurements 25
      3.5.1. Methane and hydrogen determination 25
      3.5.2. Acetate determination 26
      3.5.3. Ammonium ion determination 26
      3.5.4. Suspended solid determination 27
      3.5.5. Chemical Oxygen Demand determination 27
      3.5.6. Bromide anion determination 28
      3.5.7. Scanning electron microscopy analyses 28
   3.6. Calculations 28
4. Results 31
   4.1. Microbial electrolysis cell (MEC) 31
      Run I: Performance of the MEC fed with a synthetic solution containing acetate as sole carbon source (bioanode potential controlled at -0.1 V *vs.* SHE) 31
      Run II: Performance of the MEC fed with a synthetic solution containing soluble organic compounds other than acetate (bioanode potential controlled at -0.1 V *vs.* SHE) 38
   4.2. Hydrodynamic characterization of the bioanode 46
   4.3. Scanning Electron Microscopy (SEM) 49
5. Discussion 51
   5.1. Effect of the anode potential on the MEC performance 51
   5.2. Effect of different substrates on MEC performance 54
   5.3. Fluidynamic analysis of the MEC 57
6. Conclusive remarks and future perspectives 61
7. Bibliography 65

## List of Figures

Figure 1.1 - Direct or mediated extracellular electron transfer mechanisms at the cathode of a bioelectrochemical system. ..... 2

Figure 1.2 - Schematics of a microbial fuel cell (MFC): at the anode, organic material from the wastewater is oxidized by electrochemically active microorganisms, which transfer the gained electrons to the electrode. Via an external circuit, the electrons are transported to the cathode, where are consumed for oxygen reduction..... 4

Figure 1.3 - Schematics of a microbial electrolysis cell (MEC): the electrons released at the anode from the oxidation of organic matter are exploited for proton reduction to hydrogen gas at the cathode. The cathodic reaction typically requires a catalyst to proceed..... 7

Figure 1.4 - Main features of conventional anaerobic and aerobic biofilm processes and electro-active biofilms in a methane-producing MEC (biomass growth was not considered in this simplified representation)..... 10

Figure 1.5 - Enhanced methane production and waste substrate removal through a coupled anaerobic digestion (AD) and methane-producing MEC: the AD liquid and gaseous effluents are further processed at the anode and the cathode of the MEC, respectively. ..... 11

Figure 3.1 - Microbial electrolysis cell design. ..... 15

Figure 3.2 - Structure of Nafion membrane. ..... 15

Figure 3.3 - Schematic overview of the MEC anode compartment. ..... 18

Figure 3.4 - Schematic overview of the MEC cathode compartment. ..... 19

Figure 3.5 – Schematic representation of the theoretical model that had the better adjustment to the tracer experiment: combination of a PFR and a CSTR with stagnant zones. ..... 20

Figure 4.1 - Potential applied to the bioanode overtime. Run I of this experimentation started on day 33, when the bioanode potential was controlled at -0.1 V *vs.* SHE. ..... 31

Figure 4.2 - Acetate concentration in the influent and effluent streams of MEC anode at different applied potentials (A). Percentage of acetate removal in the MEC at different applied potentials (B). The dashed line and the lighter points represent the data that is not reviewed in this study; the same succeed for the following graphics. ..... 33

Figure 4.3 - Current generation by the activated sludge at different anode potentials. The dotted line represents the data collected on the first 33 days of the major run, and the continuous line represents the data referred to Run I. ..... 34

Figure 4.4 - Coulombic efficiency over time at different studied potentials..... 34

Figure 4.5 - Time course of cumulative methane and hydrogen production with the anode potential controlled at different values. In particular, Run I refers to the period that occurs from day 33 until day 85, when the anode potential was controlled at -0.1 V *vs.* SHE (A). Rate of methane and hydrogen production over time (B)..... 35

Figure 4.6 - Methane and hydrogen cathode capture efficiency during the MEC operation period..... 36

Figure 4.7 - Measured ammonium nitrogen concentration at the cathode and in both influent and effluent anode streams during the MEC operation period. ..... 38

Figure 4.8 - Current generation by the activated sludge at different anode potentials and OLR, before and during Run II. ..... 39

Figure 4.9 - Acetate concentration in the influent and effluent streams of the MEC anode during Run II (A). Percentage of acetate removal in the reactor during Run 2 (B). ..... 40

Figure 4.10 - COD concentration in the influent and effluent streams of the MEC anode during Run II (A). Percentage of COD removal in the reactor during Run II (B). ..... 41

Figure 4.11 - Time course of anode's coulombic efficiency in the MEC, referred to the total COD depletion. ..... 42

Figure 4.12 - Time course of the cumulative methane and hydrogen production throughout Run II (A). Rate of methane and hydrogen production over time (B). ..... 43

Figure 4.13 - MEC cathode capture efficiency during the Run II. ..... 44

Figure 4.14 - Ammonium nitrogen concentration at the anode (influent and effluent streams) and cathode chamber of the MEC, throughout Run II. ..... 44

Figure 4.15 - Hydrodynamic response of the bioanode to tracer step-input as F(t) function at the end of Run I. The dashed curve represents the F(t) theoretical curve of the proposed combination of ideal reactors. ..... 47

Figure 4.16 - Hydrodynamic response of the bioanode to tracer step-input as F(t) function and normalized current generation after Run II. The dashed curve represents the F(t) theoretical curve of the proposed combination of ideal reactors. ..... 48

Figure 4.17 - Scanning electron micrographs, near the inlet stream of the MEC: (A) unused graphite granule, (B) bacteria growing on a bioanode graphite granule, (C) bacteria growing on a biocathode graphite granule and (D) the anodic side of Nafion membrane. ..... 50

Figure 4.18 - SEM images of graphite granules taken near the outlet of the MEC: (A) anode and (B) cathode. ..... 50

Figure 5.1 - Performance of the MEC as a function of the set anode potential in terms of: generated electric current, acetate removal efficiency, and coulombic efficiency. ..... 52

Figure 5.2 - Performance of the MEC as a function of the set anode potential in terms of average methane production rate and cathode capture efficiency. ..... 53

Figure 5.3 - Performance of the MEC as a function of the set anode potential in terms of energy efficiency and acetate removal efficiency. ..... 54

Figure 5.4 - Performance of the MEC anode with respect to the type of substrate. ..... 55

Figure 5.5 - Performance of the MEC with respect to substrate type in terms of average methane production rate and cathode capture efficiency. ..... 56

Figure 5.6 - Performance of the MEC with respect to substrate type in terms of energy efficiency and acetate removal efficiency. ..... 57

Figure 5.7 - Visible lack of graphite in the reactor chamber. ..... 58

Figure 5.8 - Trend of the three tracer experiments carried out throughout the MEC operation.. 59

## List of Tables

Table 3.1 - Anodic and cathodic reactions occuring in the MEC. ..... 29

Table 4.1 - Steady-state nitrogen mass balance of the MEC. ..... 37

Table 4.2 - Summary of the main parameters of the MEC operation throughout Run I and Run II. ..... 45

Table 4.3 - Parameters estimated for the theoretical model adjusted to the first tracer experiment. ..... 46

Table 4.4 - Parameters estimated for the theoretical model adjusted to the second tracer experiment. ..... 48

Table 5.1 - Operating conditions and main results of the three performed tracer experiments for the MEC. ..... 58

## List of Abbreviations

| | |
|---|---|
| **AD** | Anaerobic digestion |
| **BES** | Bioelectrochemical systems |
| **CCE** | Cathode capture efficiency (%) |
| **CE** | Coulombic efficiency (%) |
| **CEM** | Célula de electrólise microbiana |
| **COD** | Chemical oxygen demand (g $L^{-1}$ $d^{-1}$) |
| **CQO** | Carência química de oxigénio (g $L^{-1}$ $d^{-1}$) |
| **CSTR** | Continuous-stirred tank reactor |
| **ECC** | Eficiência de captura catódica (%) |
| **FID** | Flame ionized detector |
| **HRT** | Hydraulic retention time (h, d) |
| **ISS** | Inert suspended solids (g $L^{-1}$) |
| **MDC** | Microbial desalination cell |
| **MEC** | Microbial electrolysis cell |
| **MFC** | Microbial fuel cell |
| **MSC** | Microbial solar cell |
| **OLR** | Organic load rate (kg COD $m^{-3}$ $d^{-1}$, gCOD $L^{-1}$ $d^{-1}$) |
| **PEM** | Proton exchange membrane |
| **PFR** | Plug-flow reactor |
| **SEM** | Scanning electron microscopy |
| **SHE** | Standard hydrogen electrode |
| **TCD** | Thermal-conductivity detector |
| **TSS** | Total suspended solids (g $L^{-1}$) |
| **VSS** | Volatile suspended solids (g $L^{-1}$) |

## Nomenclature

| | |
|---|---|
| $A_c$ | Cross-sectional area ($cm^2$) |
| $C_0$ | Initial concentration of the conservative tracer (g $L^{-1}$) |
| $C(t)$ | Concentration of the tracer at time *t* (g $L^{-1}$) |
| $C_{I,1,2,O}$ | Concentration in the respective streams of the PFR/CSTR model (g $L^{-1}$) |
| $\overline{C}_1$ | Laplace transform of the outlet concentration of the PFR |
| $\overline{C}_I$ | Laplace transform of the inlet concentration of the PFR |
| $\overline{C}(x,s)$ | Laplace transform of the concentration of the PFR |
| $D_{ax}$ | Dispersion coefficient ($cm^2$ $s^{-1}$) |
| F | Faraday constant (96 485 coulomb $mole^{-1}$) |
| $F$ | Molar flow (mol $s^{-1}$) |
| $i$ | Current (ampere) |
| i(*t*) | Current value at time *t* |
| $i_{max}$ | Maximum value of current achieved |
| $L$ | Distance (cm) |
| $meq_i$ | Cumulative charge (milliequivalents) |
| $N_{Anode,\ in}$ | Quantity of nitrogen in the inlet stream of the anode (mgN $d^{-1}$) |
| $N_{Anode,\ out}$ | Quantity of nitrogen that comes out the reactor (mgN $d^{-1}$) |
| $N_{Anode \rightarrow Cathode}$ | Quantity of nitrogen that flows from the anode to the cathode (mgN $d^{-1}$) |
| $P_1$ | Weight of the filter (mg) |
| $P_2$ | Weight of the filter with sample (mg) |
| $P_3$ | Weight of the filter with sample after treated (mg) |
| $Pe$ | Peclet number |

| | |
|---|---|
| $Q$ | Electric charge (coulomb) |
| $r_{CH4}$ | Methane production rate (meq $d^{-1}$, L $L^{-1}$ $d^{-1}$) |
| $s$ | Independent variable in the Laplace domain |
| $t$ | Time (s) |
| $u$ | Linear flow rate (cm $s^{-1}$) |
| $v$ | Volumetric flow rate (L $s^{-1}$) |
| $x$ | Dimensionless distance |

## Greek Letters

| | |
|---|---|
| $\alpha$ | Fraction of the CSTR volume |
| $\beta$ | Fraction of the stagnant zone volume |
| $\gamma$ | Fraction of the flow rate |
| $\Delta G_{CH4}$ | Gibbs free energy of methane oxidation (kJ $mol^{-1}$) |
| $\Delta V$ | Potential difference (V) |
| $\varepsilon_0$ | Bed porosity |
| $\eta_E$ | Energy efficiency (%) |
| $\theta$ | Dimensionless time |
| $\lambda$ | Auxiliary variable |
| $\tau$ | Space time (s) |
| $\varphi$ | Molar flux (mol $s^{-1}$ $cm^{-2}$) |

# 1. Literature Review

A sustainable society requires an alternative to fossil fuels and lower levels of generated pollution. Currently the annual world's energy demand is estimated at 13 terawatts (TW), and an additional 10 TW are estimated to be needed by 2050, to meet the demands of projected world population growth and lift the developing world out of poverty while also preserving the current lifestyles of developed countries (Pant et al. 2011). Energy sources can be divided into fossil sources (oil, coal and gas), nuclear power and renewable sources (e.g. sun, wind, biomass, hydropower and geothermal power). The fossil sources provide approximately 80 % of the total energy demand, nuclear energy 7 % and renewable sources around 13 % (Goldemberg & Johansson 2004). Considering the energy sources used for electricity generation, 63 % of the electricity is produced from the fossil sources (coal, oil and natural gas), 14 % from nuclear energy, 16 % from the hydro renewable sources, and the remaining 7 % from the non-hydro renewable sources (wind, biomass, solar, geothermal and marine) (IEA 2010). With the amount of fossil resources becoming more limited and the need to control greenhouse gas effects due to carbon dioxide emissions resulting from their usage, an intense research for sustainable and carbon-free or carbon-neutral energy carriers[1] is being driven worldwide (Schiermeier et al. 2008).

Notwithstanding, our societies are also producing an increasing quantity of organic waste, such as industrial and agricultural wastewaters. The objective of traditional wastewater treatments with biotechnological processes is the elimination of polluting compounds to generate a liquid, gaseous or solid residue that can be released in a natural environment without negative ecological effects. As these wastewaters contain high levels of easily degradable organic material, they are ideal candidates for bioprocessing, switching the paradigm of these waste streams from pollutant to raw material, as they can provide bioenergy or biochemicals (Agler et al. 2011; Kleerebezem & van Loosdrecht 2007; Angenent et al. 2004). In the recent years, innovative technologies have been developed with the goal of combining traditional elements from environmental biotechnology for the treatment of waste streams, with industrial biotechnology that is aiming for the generation of valuable products. Biotechnological processes catalyzed by microorganisms have been intensively developed towards these objectives, and bioelectrochemical systems (BESs) appear as a promising alternative for treating different types of wastewater and simultaneously fit the demands of this growing energy society.

[1] Energy carrier – is a transmitter of energy. They occupy intermediate steps in the energy-supply chain between primary sources and end-use applications.

## 1.1. Bioelectrochemical Systems

Bioelectrochemical systems are an innovative and attractive technique that combines bacterial metabolism and electrochemistry for wastewater treatment. According to the definition of conventional electrosynthesis, microbial electrosynthesis was defined as 'the microbially catalyzed synthesis of chemical compounds in an electrochemical cell' (Rabaey & Rozendal 2010). BESs employ solid state electrodes to directly or indirectly stimulate and control microbial metabolism. These systems consist of an anode, a cathode and, usually, a membrane separating the two. At the anode, an oxidation reaction occurs, and the electrode works as electron acceptor, whereas at the cathode the electrode serves as electron donor for the reduction reaction. At least one of the anodic or cathodic reactions is microbially catalyzed. Those electrodes are surrounded by an electrolyte – the fluid that contains the reactants and/or products – which is denominated as anolyte or catholyte attributed by the respective compartment.

The main characteristic of electro-active bacteria is their ability to transport electrons inside and outside the cell; this process of electron transfer can be either direct or indirect (Figure 1.1). The direct mechanism of electron transfer relies on physical contact between the bacterial cell and the electrode. This interaction is established by cytochromes or other redox active components (such as pili or nanowires) located on the outer membrane of the microorganisms (Lovley 2008; Reguera et al. 2005). The indirect mechanism involves the redox cycling of electron shuttles, which transport the electrons from the cell to the electrode. These electron shuttles can be distinguished in exogenous or endogenous.

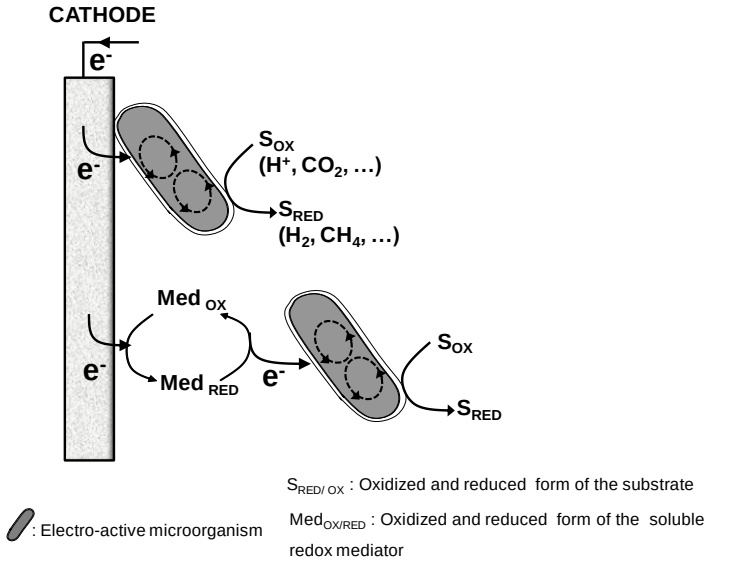


Figure 1.1 - Direct or mediated extracellular electron transfer mechanisms at the cathode of a bioelectrochemical system (Villano, Aulenta & Majone 2012).

Exogenous mediators can be humic acids and sulfur species, that are naturally present in the cells, or can be externally added, like viologens and quinones (Aulenta et al. 2007; Aulenta et al. 2010). Endogenous electron shuttles are produced as secondary metabolites by microorganisms, such as flavins (Von Canstein et al. 2008) and phenazanines (Venkataraman et al. 2010; Rabaey et al. 2005).

Extensive research has been done to elucidate both mechanisms, where iron-reducing bacteria such as *Shewanella* spp. and *Geobacter* spp. are mainly used as model microorganism. Nevertheless, an increasing number of publications shows that a wide variety of bacteria (other than iron reducers) can also participate in extracellular electron transfer processes. Indeed, the analysis of mixed microbial communities in BESs revealed a high degree of diversity and pointed at microbial interactions motivating the electron flow (Kiely et al. 2011; Logan 2009). As an example, Kiely et al. have studied the community profiles of electro-active microbial consortia in BESs fed with different fermentable substrates (e.g., ethanol, acetate, cellulose, wastewater). The conclusions revealed the existence of syntrophic partnerships between fermentative bacteria converting the organic substrates and electro-active bacteria (typically *Geobacter* species) oxidizing fermentation end products, allowing the rapid and complete conversion of complex substrates (as wastewater streams) into valuable by-products.

Based on their mode of application and operation, BESs can be sub-divided into microbial fuel cells (MFCs), microbial electrolysis cells (MECs), microbial desalination cells (MDCs) and microbial solar cells (MSCs). In fact, the term MXC was recently created for these systems, where the X stands for the different types and applications of the microbial cell (Harnisch & Schröder 2010). The last two types are out of the scope of this research and have been described in detail by Rosenbaum et al. 2010, and Mehanna et al. 2010 plus Jacobson et al. 2011, respectively. Due to their versatility, high level of control over the biological reactions and capacity to sustain a wide range of biochemical processes, BESs hold a great potential for application in environmental biotechnology, and particularly for bioenergy generation (Villano, Aulenta & Majone 2012).

### 1.1.1. Microbial Fuel Cell – electricity generation

The most extensive studied BES is the microbial fuel cell, which is commonly considered as a sustainable technology for electricity generation and simultaneous wastewater treatment (Logan et al. 2006; Du et al. 2007). A typical MFC consists of an anodic chamber and a cathodic chamber separated by an ion exchange membrane. At the anode, microorganisms catalyze the oxidation of organic or inorganic substrates using the electrode as electron acceptor. The

electrons flow from the anode to the cathode through an external electric circuit containing a resistor or a load (i.e., the device being powered). Generally, the electrons that reach the cathode combine with protons, which diffuse from the anode through the membrane, and oxygen, provided from air; hence, the resulting product of this reaction is water (Min & Logan 2004; H. J. Kim et al. 2002) (Figure 1.2). The ideal performance of an MFC depends on the electrochemical reactions that occur between the organic substrate at a low potential, such as glucose, and the final electron acceptor with a high redox potential, such as oxygen (Rabaey & Verstraete 2005). In addition, the high oxygen availability in the environment makes it the most sustainable electron acceptor. However, to achieve a sufficiently high oxygen reduction rate at the cathode, platinum-, cobalt- and iron-based materials are frequently used as catalysts (S. Cheng et al. 2006; Zhao et al. 2005).

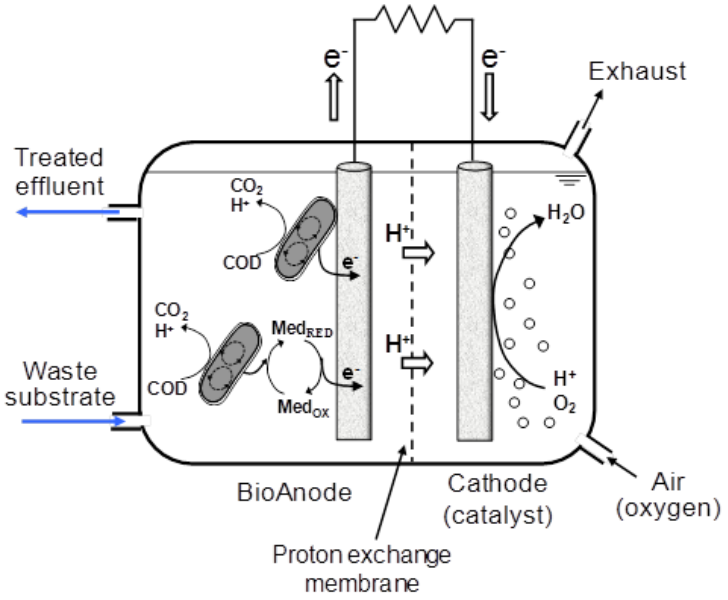


Figure 1.2 - Schematics of a microbial fuel cell (MFC): at the anode, organic material from the wastewater is oxidized by electrochemically active microorganisms, which transfer the gained electrons to the electrode. Via an external circuit, the electrons are transported to the cathode, where are consumed for oxygen reduction (Villano, Aulenta & Majone 2012).

In relation to the electron flow in the system, it is known that the movement of electrons to the cathode must be compensated by transport of an equal amount of positive charge to the cathode chamber, in order to sustain the electroneutrality of the system. Therefore, the proton exchange membrane (PEM) is one of the most critical components in the MFC, as it physically separates the anode and the cathode compartments while allowing protons to pass through to the cathode. The Nafion 117 membrane (Dupont Co., USA) is one of the most frequently used PEMs in MFCs. It consists of a hydrophobic fluorocarbon backbone to which hydrophilic sulfonate groups ($-SO_3^-$) are attached (Mauritz & Moore 2004). The high cation conductivity of Nafion®

can be explained from the high concentration of these negatively charged sulfonate groups in the membrane ($[-SO_3^-] \approx 1.13$ mol $L^{-1}$) (Rozendal 2006). However a number of problems associated with these membranes still exist, namely the oxygen leakage from cathode to anode, substrate loss, cation transport and accumulation rather than protons, and biofouling (Chae et al. 2008).

Several substrates have been investigated as possible energy sources to generate electrical power in MFCs. Among them are carbohydrates (e.g., glucose, sucrose, cellulose and starch), volatile fatty acids (e.g., formate, acetate and butyrate), alcohols (e.g., ethanol and methanol), amino acids, proteins and even inorganic components (J. R. Kim et al. 2007; Heilmann & Logan 2006; Logan et al. 2005; Liu, S. Cheng, et al. 2005). Furthermore, a wide range of more complex feeds, containing a large variety of different readily and non-readily degradable molecules such as domestic wastewaters, brewery wastewater or the effluent of anaerobic digesters have also been demonstrated to sustain electrical power generation in MFCs (Pant et al. 2010; Min et al. 2005; Liu et al. 2004). Nonetheless, the nature of the substrate affects both the composition of the bacterial community and the MFC performance, which means the power density and the coulombic efficiency (CE) of the system. From the perspective of energy recovery as power in a MFC, high CE is desirable. Moreover, bacteria that produce high CEs will have low biomass yields, as the electrons from the substrate are used to produce current. CEs as high as 96.8 % have been reported, suggesting that only 3.2 % or less of the electrons could have gone into biomass production (Bond & Lovley 2003).

In order to assess the practical viability of MFCs, their performance in terms of wastewater treatment capacity (i.e., substrate conversion rate), and bioenergy generation potential (i.e., electrical power generation) can be compared to that of conventional anaerobic digestion systems. For instance, high-rate anaerobic reactors can be operated at organic loading rates (OLRs) as high as 25 kgCOD $m^{-3}$ $d^{-1}$; in a MFC the same substrate conversion rate would correspond to a volumetric current density of around 3500 A $m^{-3}$ (considering that 1 kgCOD can be theoretically converted into approximately $12\times10^6$ Coulombs). So far, the highest current density achieved is 595 A $m^{-3}$ (Rabaey et al. 2010).

To calculate power generation of anaerobic digestion, it should be first considered that approximately 1 kWh of usable electrical energy is obtained from the conversion of 1 kgCOD into methane. During the conversion of biogas into electricity via cogeneration, up to other 3 kWh are typically recovered as heat, used to warm up the digester, or are lost (Pham et al. 2006). By considering a high-rate digester that operates at an OLR of 25 kgCOD $m^{-3}$ $d^{-1}$, the resulting volumetric power density would be around 1 kW $m^{-3}$. So far, in spite of the great scientific advancement that have been made during the last decade, the maximum reported

power densities of MFC typically stand around 0.1 kW $m^{-3}$, largely due to various losses, mainly deriving from mass transport and activation limitations, which limit the energy efficiency of the system (Villano, Aulenta & Majone 2012).

Aside the existing limitations and the currently higher installation costs, the MFC technology holds some specific advantages over anaerobic digestion, e.g. the applicability for the treatment of dilute wastewater, the possibility to operate at low temperatures, no need for gas handling and/or cleaning, and the greater control over biochemical conversion processes. All these features make these systems attractive for specific application niches (Pham et al. 2006). The power outputs of MFCs have improved rapidly over the last decade by varying the design, the operating conditions, optimizing configurations and also the biocatalyst utilized. Nevertheless, the electric power could not be the only valuable product obtained from MFCs. In reality, electrons resulting from the organic carbon oxidation can potentially be exploited at the cathode for the generation of reduced value-added products, like hydrogen, as it succeeds in microbial electrolysis cells. The co-production of a chemical product, besides the electric power, would provide considerably higher economic and environmental benefits, as stated by Foley et al. (2010).

### 1.1.2. Microbial Electrolysis Cell – hydrogen generation

Microbial electrolysis cells are a relatively new BES which exploits the catalytic activity of microorganisms to convert the chemical energy of wastewater directly into hydrogen gas (Rozendal et al. 2006; Liu, Grot, et al. 2005). Subsequently the purpose of these systems is twofold: the efficient purification of wastewater and high yield hydrogen production (Sleutels et al. 2009). Such devices are based on a similar approach to MFC, consisting of two compartments separated by an ion exchange membrane: the anode, where the electro-active microorganisms oxidize organic or inorganic substrates using the electrode as terminal electron acceptor (Rabaey & Rozendal 2010); and the cathode, where the electrons (released at the anode) reduce protons to $H_2$ in the presence of a suitable catalyst (Figure 1.3). The anode compartment design is similar for both MEC and MFC, but the main difference between these bioelectrochemical systems is that the MEC has an anaerobic cathode, allowing the hydrogen evolution reaction rather than electricity. Since the final product is hydrogen, the cathode architecture must be modified to collect the produced gas (Villano, Aulenta & Majone 2012). Nevertheless, the potential generated from microbial substrate oxidation requires to be boosted with an external power supply. Being acetate used as a model compound for the biocatalyzed electrolysis an applied voltage of 0.14 V is required, in theory (Rozendal et al. 2006), in order to

overcome the thermodynamic barrier and to drive the cathodic reaction at high rates (Villano et al. 2011).

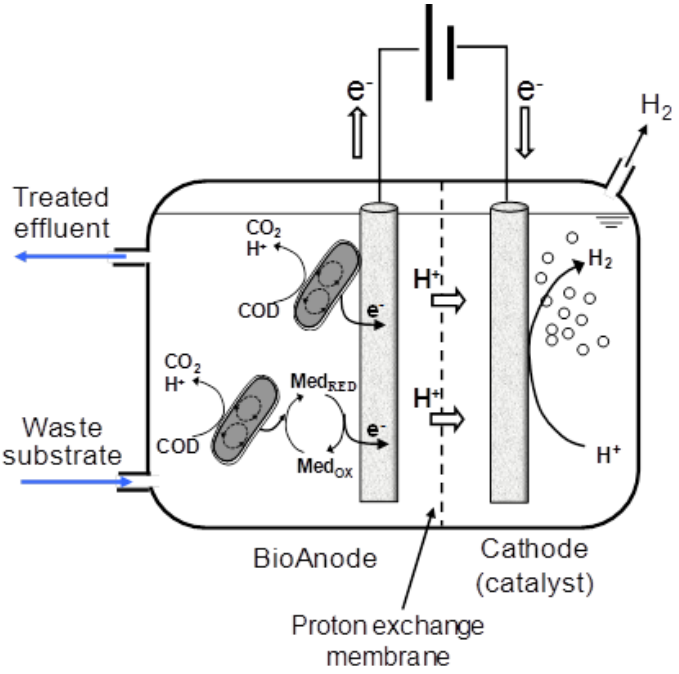


Figure 1.3 - Schematics of a microbial electrolysis cell (MEC): the electrons released at the anode from the oxidation of organic matter are exploited for proton reduction to hydrogen gas at the cathode. The cathodic reaction typically requires a catalyst to proceed (Villano, Aulenta & Majone 2012).

In practice, due to microorganisms activity and other losses in the cell, larger voltages (0.2-1.0 V) must be applied (Rozendal et al. 2006). Still the required voltage is significantly lower than the one needed for hydrogen production through water electrolysis (1.6-2.0 V) (Zeng & Zhang 2010).

The requirement of noble metal (e.g., Pt-based) catalysts to enhance the rate and efficiency of the cathodic reaction is one of the disadvantages of MEC, since these catalysts are expensive and susceptible to poisoning. Alternative low-cost cathodic catalysts, including carbon felt, stainless steel and nickel alloys, have also been investigated, though they often exhibit insufficient chemical stability and/or reactivity at neutral pH for efficient MEC operation (Call et al. 2009; Selembo et al. 2009).

The requirement of cheaper and more sustainable cathodes has motivated the research into the development of microbial biocathodes (Rozendal et al. 2008; Clauwaert, Van der Ha, et al. 2007), where the microorganisms are the electrocatalytic agents of the target cathodic reaction. The main advantages of microbial biocathodes include self-regeneration of the catalyst, low cost, they can effectively operate under neutral pH conditions and are not susceptible to corrosion. Furthermore, due to their metabolic versatility and specificity, microbial biocathodes

offer the potential to produce a variety of value added products. As an example it has been demonstrated that microbial biocathodes can be employed in oxygen reduction (Clauwaert, Van der Ha, et al. 2007), nitrate and fumarate reduction (Clauwaert, Rabaey, et al. 2007; Gregory et al. 2004), and bioremediation processes (Aulenta et al. 2011; Aulenta et al. 2009). The MECs set with this type of cathodes can also be employed to produce methane from carbon dioxide reduction (Villano et al. 2010; S. Cheng et al. 2009). This reaction could exploit the electrons and the carbon dioxide released at the anode from the microbial oxidation of organic matter contained in a waste stream, as will be discussed in the following section.

## 1.2. Coupling organic substrate removal to methane production

Renewable biomethane is typically produced by methanogens from a few substrates such as acetate, formate and hydrogen gas in anaerobic digesters (Wall et al. 2008). Recently, MEC have also been confirmed as a new technique to produce methane. In a methane-producing MEC, the electrons released from the anodic oxidation of organic matter are used for $CO_2$ reduction into methane, by using a suitable chemical or biological catalyst. The latter include methanogenic consortia, similar to anaerobic digestion (AD) (Villano et al. 2011; Villano et al. 2010; S. Cheng et al. 2009). For microbial biocathodes two distinct mechanisms of methane production have been identified: direct reduction of $CO_2$ (Equation 1.1) with methanogens accepting electrons from a polarized cathode,

$$CO_2 + 8H^+ + 8e^- \rightarrow CH_4 + 2H_2O$$

Equation 1.1

and indirect reduction of $CO_2$ (Equation 1.2 and 1.3) with methanogens using $H_2$ gas as electron donor in their metabolism,

$$2H^+ + 2e^- \rightarrow H_2$$

Equation 1.2

$$CO_2 + 4H_2 \rightarrow CH_4 + 2H_2O$$

Equation 1.3

Methane production via direct reduction is considered the most energy-efficient process, as the standard potential of hydrogen production via indirect mechanism (-0.410 V *vs.* SHE – standard hydrogen electrode) is lower than that of direct methane production (-0.244 V *vs.* SHE).

Up till now, few studies have investigated this application of MEC technology; for that reason fundamental information concerning the optimal operating conditions and achievable

performances is rather limited. Besides, as it is a relatively new technique, the process needs to be examined and evaluated on the basis of performance indicators, such as applied voltage, overall process efficiency, energy requirement and production rates. In a recent study (Villano et al. 2011), a fully biological MEC, consisting of a *Geobacter sulfurreducens*-enriched bioanode and a methane-producing biocathode, was described. The MEC was successfully started up by sequentially controlling the cathode and the anode potentials at values that are favorable to the establishment of an active methanogenic biocathode (i.e. -0.850 V *vs.* SHE) and acetate-oxidizing bioanode (+0.500 V *vs.* SHE). The highest methane production rate (approximately 0.05 $m^3$ $m^{-3}$ $d^{-1}$) was obtained by controlling the cathode at -0.850 V *vs.* SHE, whereas the value achieved with the MEC being operated at a controlled anode potential of +0.500 V *vs.* SHE was three times lower. However, similar to other biocathode studies, the performance of the system was found to be primarily limited by the concentration of biomass in both compartments, suggesting that a possible strategy to optimize the process involves saturating the electrodic surfaces with microorganisms (Villano, Aulenta & Majone 2012).

A subsequent study (Villano et al. 2013), where the bioanode was controlled at +0.200 V *vs.* SHE, demonstrated a substrate removal efficiency of 94 % and the current stabilize at around 110 mA; the close correlation between current generation and acetate consumption clearly indicated the ability of the inoculated sludge to use the graphite anode, poised at +0.200 V, as terminal electron acceptor for electrochemical substrate oxidation. Concerning the average energy efficiency, a parameter that takes into account the voltage difference between the anode and the cathode potentials, it accounted for 75 %. In order to try to obtain a net positive energy recovery, it is suggested to investigate the MEC performance controlling the anode at less-positive potentials, without adversely affecting the substrate removal efficiency.

A methane-producing MEC combines features that are typical of conventional aerobic biofilm processes, like the possibility to oxidize diluted streams, with those of conventional anaerobic biofilm processes, as the possibility of energy recovery in the form of methane (Figure 1.4).

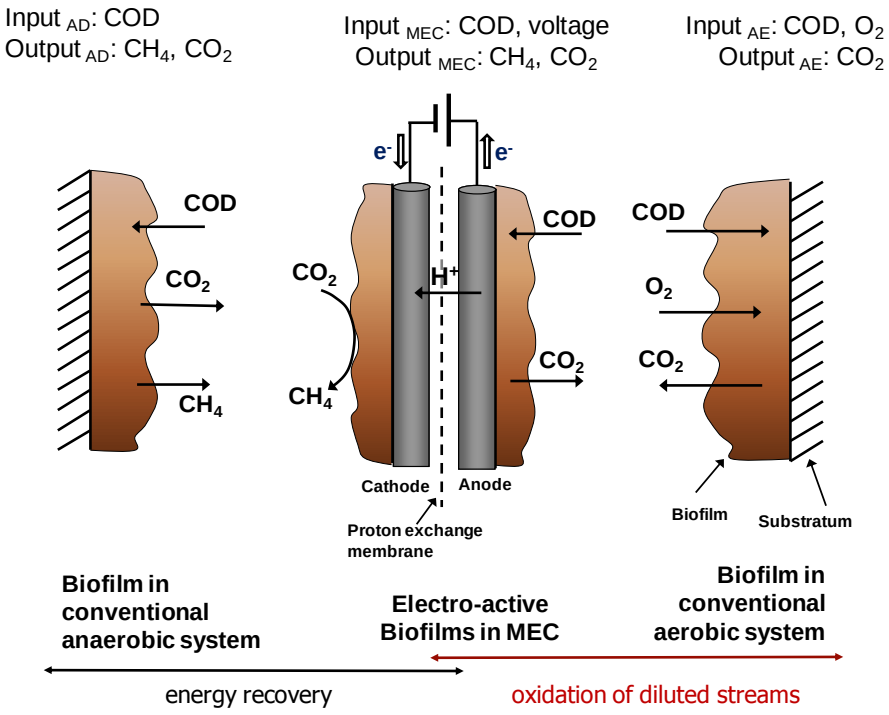


Figure 1.4 - Main features of conventional anaerobic and aerobic biofilm processes and electro-active biofilms in a methane-producing MEC (biomass growth was not considered in this simplified representation) (Villano, Aulenta & Majone 2012).

Even though AD is an outstanding competitor, since it is a well-established and effective biotechnology, this process potentially holds some specific advantages compared with a traditional AD process; namely the physical separation of the organic matter oxidation from the methane generation could in principle allow the production of a biogas richer in methane, and the protection of methanogenic consortia against inhibitory compounds possibly contained in the waste stream. Moreover, less thermal energy (if any) is needed to control the temperature of the cathode because the waste stream does not need to be warmed up, being processed only at the anode side, and analogously to other BESs, low strength wastewater (< 1 kgCOD $m^{-3}$) can also be treated. In this context, it has been also proposed to operate a MEC in series to a conventional anaerobic digester, by removing the residual organic matter contained in the digestate, which would otherwise represent a disposal burden and a waste of energy. In order to meet stringent effluent discharge limits, AD systems require a "polishing" post-treatment step, which is typically achieved in energy-intensive activated sludge systems, where the residual organic matter is aerobically oxidized to carbon dioxide and water, with concomitant production of considerable amounts of sludge.

The use of MEC in series to fermentative or methanogenic bioprocesses is particularly attractive because AD effluents primarily consist of diluted organic acids, that are ideal substrates for

electro-active bacteria, and so can be further removed, to avoid recirculation of AD effluent into the wastewater treatment plant. At the same time, continuously bubbling the biogas produced from AD (which typically consists of carbon dioxide (25-45 vol%) and methane (75-55 vol%)) through the MEC cathode would supply carbon dioxide for methane production, which could be a strategy to add energetic and economic value to the AD biogas, by increasing its methane content. A schematic diagram showing a possible integration opportunity for AD and methane-producing MEC is shown in Figure 1.5. Hence, coupling AD and MEC in the sludge line of a wastewater treatment plant will also contribute to decrease net sludge production while increasing the energy recovery (Villano, Aulenta & Majone 2012).

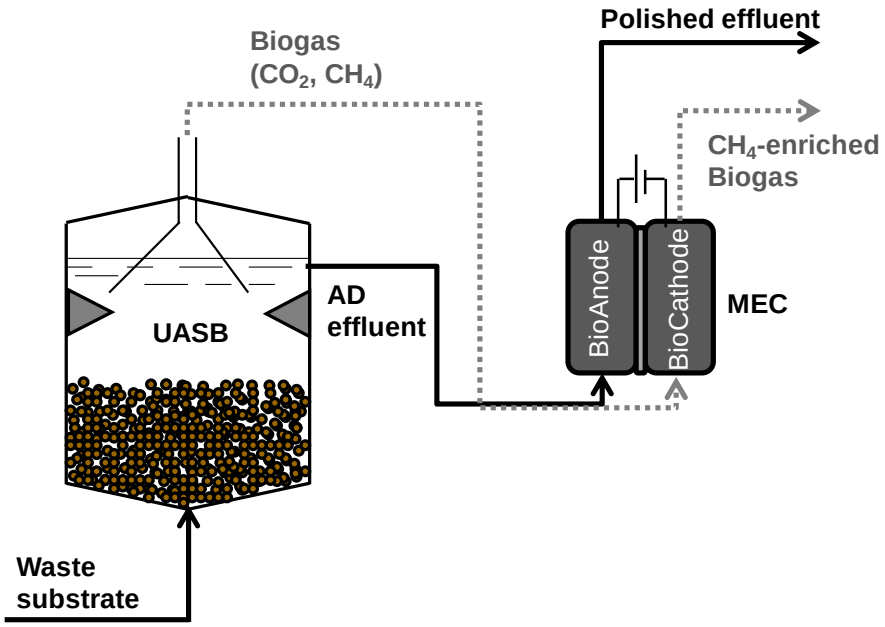


Figure 1.5 - Enhanced methane production and waste substrate removal through a coupled anaerobic digestion (AD) and methane-producing MEC: the AD liquid and gaseous effluents are further processed at the anode and the cathode of the MEC, respectively (Villano, Aulenta & Majone 2012).

## 2. Research objectives

The main objective of this research is the evaluation of the performance of a fully biological two-chamber microbial electrolysis cell (MEC) in terms of organic matter oxidation (at the anode), and methane production (at the cathode). Considering that previous studies were mostly done at anode potential +0.2 V *vs.* SHE (standard hydrogen electrode) or higher and by using acetate as the only substrate, this dissertation intends to study the performance of the MEC:

- Operated at a lower anode potential (i.e. -0.1 V *vs.* SHE);
- fed by either acetate or substrates with different complexities.

In order to accomplish the target objectives, the research plan has been organized as follows:

- The anode had been previously inoculated with an activated sludge, whereas the cathode chamber inoculum was an anaerobic sludge (containing methanogenic microorganisms).
- Initially, the MEC performance was studied by continuously feeding the anode chamber with an acetate solution as substrate, at an applied organic load rate of 1.08 gCOD $L^{-1}$ $d^{-1}$ (Run I). During this Run the anode potential was controlled at -0.1 V *vs.* SHE by means of a potentiostat. The performance of the system was evaluated in terms of substrate removal, coulombic efficiency (CE), cathode capture efficiency (CCE), methane and hydrogen production rates, and energy efficiency ($\eta_E$).
- The results of Run I were then compared with results from previous studies, carried out with the same conditions but at different anode potentials. This allowed to evaluate the effect of the anode potential on the MEC performance.
- Subsequently, with the purpose of studying the effect of substrate composition, the feeding solution was replaced by a synthetic solution containing soluble organic compounds other than acetate (Run II), with a similar applied organic load rate (0.93 gCOD $L^{-1}$ $d^{-1}$), and all other conditions being the same. Likewise the performance of the system was evaluated with the same parameters as Run I.
- At the end of each run, tracer experiments were performed in order to analyze the fluid dynamics of the MEC.
- Furthermore, to acquire microscopy analyses, the reactor was disassembled and samples of graphite granules were collected from the anode and cathode compartments, as well as from the membrane.

# 3. Materials and methods

## 3.1.Microbial electrolysis cell design and setup

The experimental setup consisted of a two-chamber microbial electrolysis cell (MEC), made of two identical Plexiglas frames, with internal dimensions of 17 cm × 17 cm × 3 cm, bolted together between two Plexiglas plates (Figure 3.1). The two chambers, that establish the anodic and cathodic compartments, were physically separated by a Nafion® 117 (Dupont Co., USA) proton exchange membrane (PEM), which allows protons and other cations to pass through from the anode chamber to the cathode one. Nafion®, a sulfonated tetrafluorethylene copolymer, consists of a hydrophobic fluorocarbon backbone (-$CF_2$-$CF_2$-) to which hydrophilic sulfonate groups (-$SO_3^-$) are attached (Mauritz & Moore 2004), as shown in Figure 3.2. The main characteristics of this membrane are: the high level of proton conductivity, explained by the presence of negatively charged sulfonate groups in the membrane, the good mechanical properties and the long-term stability as the membrane shows a lifetime of more than 10,000 h (Appleby & Yeager 1986). Prior to being used, the PEM was pre-treated by boiling successively in $H_2O_2$ (3%, v/v), distilled water, 0.5 M $H_2SO_4$, and finally in distilled water again, for 2 h each.

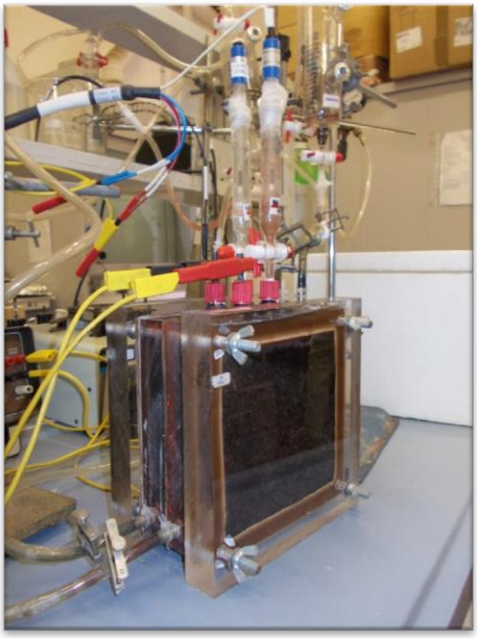

Figure 3.1 - The microbial electrolysis cell.

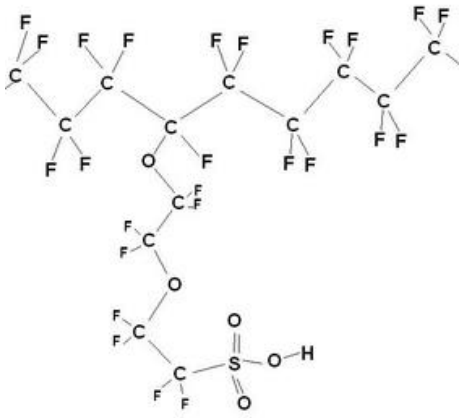

Figure 3.2 - Structure of Nafion membrane.

In the chambers were four diaphragm in plexiglass (two per each compartment, with 13 cm × 3 cm dimensions) to force a preferential liquid flow pathway across each chamber (see Figure 3.3 and Figure 3.4).

The reactor was designed to operate with three electrodes: the working electrode, the reference electrode and the counter electrode. Both working and counter electrode were composed by graphite granules filling each chamber. The electrical connections to the potentiostat (BioLogic VSP, Grenoble, France) were guaranteed by means of a graphite rod (5 mm diameter and 100 mm length, Sigma-Aldrich, Italy) placed in each compartment. A KCl saturated Ag/AgCl reference electrode (+0.199 V *vs.* standard hydrogen electrode, SHE) (Amel s.r.l., Milan, Italy) was also placed in both the anodic and cathodic compartments, in contact with the graphite granules to measure or control the potential of individual electrodes. Each reference electrode was placed close to the working or counter electrode, in order to reduce the ohmic loss and make the potential measurement and control as accurate as possible. The potential of the working electrode (anode) was controlled at -0.1 V *vs.* SHE by means of the potentiostat; whereas the potential of the counter electrode (cathode) was measured by means of a resistor.

Prior to being used, the graphite rods were treated for 1 h in a 37% HCl solution, subsequently submerged for 24 h in a HCl (1 M) solution and then for 24 h in 1 M NaOH solution. This process was repeated for two times and then the rods were thoroughly washed with distilled water. The purpose of this treatment was to remove any metallic oxides and eliminate potential organic residues from the graphite material. Prior to being used, the graphite granules were activated by means of a washing process of 3 cycles, being submerged for 24 h in 37% HCl, to remove metals from the surface, and then for 24 h in a NaOH (1 M) solution. The washing process was repeated three times and then the granules were thoroughly washed with distilled water and dried at 100 ºC. The intent of this treatment was to eliminate any potentially catalytic foreign compounds from the graphite material. By killing all microorganisms, this treatment also eliminated any potential biocatalyst that could affect the electrode performance (Freguia et al. 2007).

Both chambers were filled with 730 g of graphite granules (El Carb 100, Graphite Sales, Inc, USA) with diameters between 2 and 6 mm, with a real density of 1.709 ± 0.025 g $mL^{-1}$ and an apparent density of 0.951 g $mL^{-1}$, giving a bed porosity ($\varepsilon_0 = V_{empty}/V_{total}$) of 48 %. Besides of offering a high electrodic surface area, the graphite grains also functioned as support material for the biofilm growth. The total empty volume of each compartment was 0.86 L.

A glass chamber, equipped with sampling ports sealed with butyl rubber stoppers and aluminum crimps, was placed in the outlet of each compartment in order to sample the headspace and the liquid phase of both anode and cathode (the total volume of the glass chambers was 290 mL and

297 mL, for the anode and the cathode compartment, respectively). In the latter case, the glass chamber was connected to a MilliGascounter (Ritter, Germany), which recorded the volume of the produced gas. The connections to the pumps for each compartment were made by means of Tygon® Laboratory Tubing R-3603, impermeable to oxygen.

### 3.2. Microbial electrolysis cell operation

The experimentation was performed with microorganisms already present in the MEC from previous operation. Specifically, the anode compartment had been inoculated with 0.2 L of activated sludge collected from a local full-scale municipal wastewater treatment plant (Roma Nord, Italy), having a biomass concentration of 1.99 $\pm$ 0.06 g $L^{-1}$ as volatile suspended solids (VSS). This inoculum was kept in anaerobic conditions, in order to use the electrode as sole external electron acceptor for the oxidation of organic matter. The cathode compartment had been inoculated with 0.05 L of anaerobic sludge from the full-scale wastewater treatment plant of Treviso (Italy), with a biomass concentration of 8.35 $\pm$ 0.88 g $L^{-1}$ as VSS. Prior to being inoculated, the anaerobic sludge was diluted in mineral medium with the necessary amount of nutrients to the microbial culture. Considering the empty volume in anodic and cathodic compartments (390 and 417 mL, respectively), the initial sludge concentration in each compartment was approximately 1 g $L^{-1}$. After inoculation, the liquid phase and headspace of both compartments were flushed for 1 h with a $N_2/CO_2$ (70:30 v/v) gas mixture in order to establish anaerobic conditions. One day after the reactor was connected to the potentiostat by controlling the anode potential at the desired value. The potentiostat also allowed measuring and recording the electrical current flowing in the system. After the inoculation the MEC had been operated for almost 80 days, mostly by controlling the anode potential at +0.2 V *vs.* SHE (Villano et al. 2013)

Throughout this research, the MEC anode was operated in continuous-flow mode by using a peristaltic pump (Figure 3.3). In each compartment the liquid phase, hereafter referred to as anolyte and catholyte, was anaerobic basal medium which contained (g $L^{-1}$): $K_2HPO_4$, 4; $NH_4Cl$, 0.125; $MgCl_2 \cdot 6H_2O$, 0.1; $CaCl_2 \cdot 2H_2O$, 0.05; 10 mL $L^{-1}$ of a trace metal solution (Balch et al. 1979) and 1 mL $L^{-1}$ of a vitamin solution (Zeikus 1977). Nevertheless, for each run the initial anolyte was substituted by the feeding solution, which contained organic components, whereas the catholyte was only the mentioned basal medium.

Initially (Run I) the feeding solution (anolyte) contained acetate as organic substrate and the following composition in g $L^{-1}$: $CH_3COONa$, 0.82; $NH_4Cl$, 0.125; $MgCl_2 \cdot 6H_2O$, 0.1; $K_2HPO_4$, 4; $CaCl_2 \cdot 2H_2O$, 0.05; 10 mL $L^{-1}$ of a trace metal solution (Balch et al. 1979), and 1 mL $L^{-1}$ of vitamin solution (Zeikus 1977). The corresponding organic load rate (OLR) was 1.08 gCOD $L^{-1}$

$d^{-1}$, being acetate the sole electron donor for the anodic culture (based on the conversion factor 1.067 gCOD g $acetate^{-1}$). In a second part of the research (Run II), the feeding solution was replaced with a more complex solution containing soluble organic compounds other than acetate, with the following composition in g $L^{-1}$: $NH_4Cl$, 0.267; $CH_3COONa$, 0.077; $KH_2PO_4$, 0.053; peptone, 0.120; yeast extract, 0.065; glucose, 0.141 and starch, 0.127. In this case, the corresponding OLR was 0.93 gCOD $L^{-1}$ $d^{-1}$. Prior to being supplied to the anode, the feeding solution was flushed with a $N_2/CO_2$ (70:30 v/v) gas mixture in order to establish anaerobic conditions. Then, pH was adjusted at values between 7.00 and 7.50 by adding 40 mL $L^{-1}$ of a $NaHCO_3$ solution (10% w/v) and the solution was transferred anaerobically inside a Tedlar® bag. The feeding flow rate was 1 mL $min^{-1}$ (1.44 L $d^{-1}$), resulting in a hydraulic retention time (HRT) of 0.60 d (referred to the empty volume of the anode compartment). The effluent of this compartment was recovered in a Tedlar® bag.

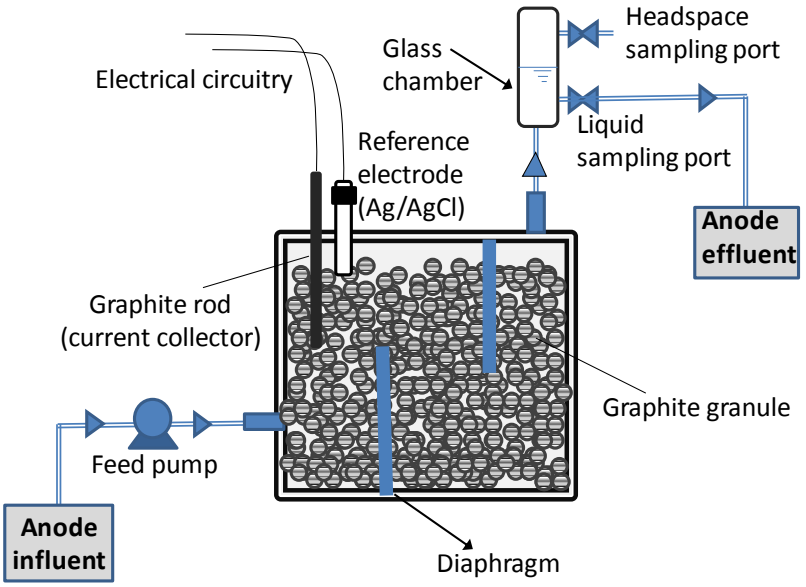


Figure 3.3 - Schematic overview of the MEC anode compartment.

The MEC cathode (Figure 3.4) was operated in a semi-batch mode with the liquid phase (catholyte) being continuously recirculated at a flow rate of 30 mL $min^{-1}$, using a peristaltic pump and Tygon® tubings, in order to prevent the establishment of products concentration gradients. Furthermore, this compartment was continuously flushed with a gas mixture of $N_2/CO_2$ (70:30 v/v), with a 10 L $d^{-1}$ flow rate, in order to control the pH and continuously supply carbonate for methane formation as well. Catholyte was the basal medium, i.e., the same composition as the anolyte but deprived of acetate or other organic compounds. Besides, a small liquid flow from the anode to the cathode compartment through the membrane was observed. Hence, to counterbalance this additional flow, it was necessary to daily remove the catholyte

collected inside the glass chamber. For Run I, the average daily withdrawn was 73.2 mL, and 51.6 mL for Run II.

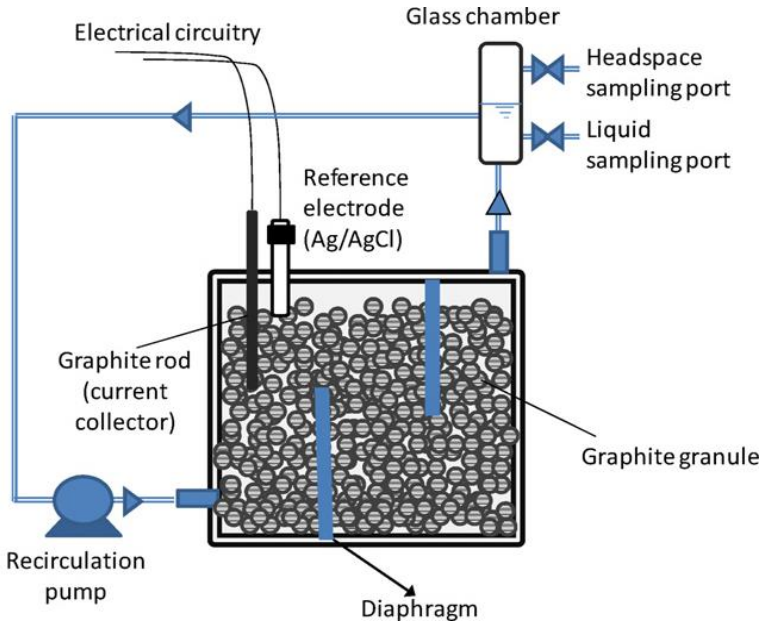


Figure 3.4 - Schematic overview of the MEC cathode compartment (Villano et al. 2011).

In order to smooth temperature variations both the influent line to the anode and the recycle line through the cathode were passed through a glass heat exchanger; typically the MEC temperature was around 24 to 26 ºC.

### 3.3. Tracer experiment

In order to characterize the hydrodynamic behavior in the anode compartment of the bioelectrochemical reactor, a tracer test was carried out for two times. Prior to performing both tests, the bioanode was fed with a mineral medium solution, in order to let current drop down to the baseline value. For the first tracer experiment, the inlet feed solution consisted of mineral medium to which was added an inert tracer (KBr) at a concentration ($C_0$) of 0.5 g $L^{-1}$ (as $Br^-$). Instead, the inlet feed solution of the second experiment was modified by adding the inert tracer to the usual acetate-containing medium, at the same concentration as before. The solution was fed into the anode in a step-input mode at a flow-rate of 0.87 mL $min^{-1}$ (1.25 L $d^{-1}$) in the first experiment and 1 mL $min^{-1}$ (1.44 L $d^{-1}$) in the second. Samples from the anode effluent during each experiment were taken at intervals of 0.5 or 1 hour. The samples were filtered (0.22 µm porosity) and stored at -4 ºC before being analyzed.

The response of the reactor to the step-input of the tracer was calculated from the non-dimensional F(*t*) curve, obtained by plotting $C(t)/C_0$ as a function of time (where C(*t*) is the $Br^-$ concentration at time *t*, and $C_0$ is its initial concentration). In the second experiment, the time profile of electric current generated from the oxidation of the acetate was also acquired and compared to the F(*t*) curve by plotting $i(t)/i_{max}$, where i(*t*) and $i_{max}$ represent the current value at time *t* and the maximum value of current achieved, respectively.

To analyze the result of the tracer experiments three theoretical models were tested. In this section, it will only be specified the equations of the theoretical model that had the better adjustment: the combination of a plug-flow reactor (PFR) and a continuous stirred tank reactor (CSTR) with stagnant zones (Figure 3.5).

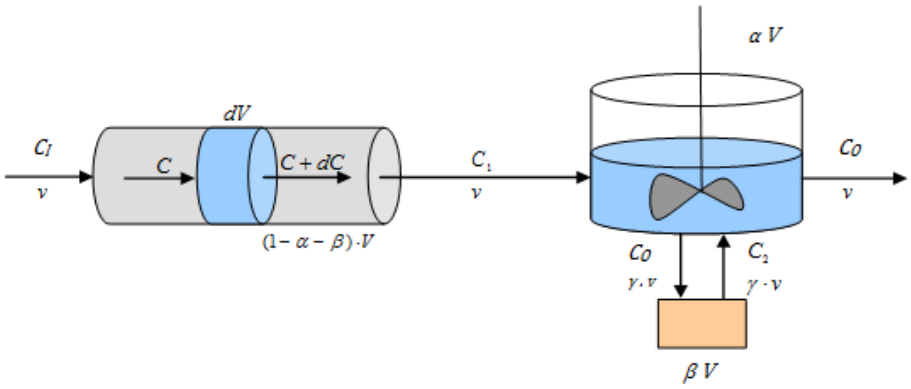


Figure 3.5 – Schematic representation of the theoretical model that had the better adjustment to the tracer experiment: combination of a PFR and a CSTR with stagnant zones.

The mole balances to the system started with the dispersion model to the tubular reactor. The balance to the volume element dV is

$$vC = v(C + dC) + \frac{dn}{dt}$$

Equation 3.1

Being $F = vC$ the molar flow, and $\varphi = \frac{F}{A_c}$ the molar flux, it cames

$$\therefore \varphi_z A_c = \varphi_{z+dz} A_c + \frac{dC}{dt} dV$$

Equation 3.2

$$\therefore \varphi_z A_c = \varphi_{z+dz} A_c + \frac{dC}{dt} A_c \, dz$$

Equation 3.3

$$\therefore \varphi_z = \varphi_{z+dz} + \frac{dC}{dt}dz$$

Equation 3.4

$$\therefore \frac{\partial C}{\partial t} + \frac{\varphi_{z+dz} - \varphi_z}{\partial z} = 0$$

Equation 3.5

$$\therefore \frac{\partial C}{\partial t} + \frac{\partial \varphi}{\partial z} = 0$$

Equation 3.6

In ideal conditions,

$$\varphi = \frac{F}{A_c} = \frac{vC}{A_c} = \frac{v}{A_c}C = uC$$

In conditions of axial dispersion $\varphi = uC - D_{ax}\frac{dC}{dz}$

$$\therefore \frac{\partial C}{\partial t} + u\frac{\partial C}{\partial z} - D_{ax}\frac{\partial^2 C}{\partial z^2} = 0$$

Equation 3.7

In order to arrive at the dimensionless group that characterize the process, let $x = \frac{z}{L}$ and $\theta = \frac{t}{\tau}$

$$\Rightarrow \frac{1}{\tau}\frac{\partial C}{\partial \theta} + \frac{u}{L}\frac{\partial C}{\partial x} = \frac{D_{ax}}{L^2}\frac{\partial^2 C}{\partial x^2}$$

Equation 3.8

As $\tau = \frac{V}{v} = \frac{A_c L}{A_c u} = \frac{L}{u}$, multiplying by $\tau$

$$\Rightarrow \frac{\partial C}{\partial \theta} + \frac{\partial C}{\partial x} = \frac{D_{ax}}{L\,u}\frac{\partial^2 C}{\partial x^2}$$

Equation 3.9

Introducing the Peclet number, that can be regarded as the ratio of

$$Pe = \frac{rate\ of\ transport\ by\ convection}{rate\ of\ transport\ by\ diffusion} = \frac{Lu}{D_{ax}}$$

Writing Equation 3.9 in terms of the Peclet number yields

$$\frac{\partial C}{\partial \theta} + \frac{\partial C}{\partial x} = \frac{1}{Pe}\frac{\partial^2 C}{\partial x^2}$$

Equation 3.10

Applying the Laplace transform $C(x,\theta) \rightarrow \bar{C}(x,s)$:

$$s\,\bar{C} + \frac{d\bar{C}}{dx} = \frac{1}{Pe}\frac{d^2\bar{C}}{dx^2}$$

$$\therefore \frac{1}{Pe}\frac{d^2\bar{C}}{dx^2} - \frac{d\bar{C}}{dx} - s\,\bar{C} = 0$$

Equation 3.11

That is an homogeneous second order differential equation, with the following characteristic polynom

$$\frac{1}{Pe}\lambda^2 - \lambda - s = 0$$

Equation 3.12

Of roots: $r_1, r_2 = \frac{1 \pm \sqrt{1+\frac{4s}{Pe}}}{2/Pe}$, the solution of the differential equation is

$$\bar{C}(x,s) = A\,e^{r_1 x} + Be^{r_2 x} = A\,e^{\frac{1+\sqrt{1+\frac{4s}{Pe}}}{2/Pe}x} + B\,e^{\frac{1-\sqrt{1+\frac{4s}{Pe}}}{2/Pe}x}$$

Equation 3.13

Considering the boundary conditions it is possible to determine the constants $A$ and $B$,

$$\begin{cases} x = 0 \Rightarrow C = C_I(0,t) \\ x \rightarrow \infty \Rightarrow C\ limited \end{cases}$$

The second condition implies that $A = 0$

$$\therefore \bar{C}(x,s) = B\,e^{\frac{1-\sqrt{1+\frac{4s}{Pe}}}{2/Pe}x}$$

Equation 3.14

The transfer function $g(s)$ is a ratio of output $C_1$ to input $C_I$, in $s$-domain:

$$g(s) = \frac{\bar{C}_1}{\bar{C}_I} = \frac{\bar{C}(1,s)}{\bar{C}(0,s)} = \frac{B\,e^{\frac{1-\sqrt{1+\frac{4s}{Pe}}}{2/Pe}}}{B} = e^{\frac{1-\sqrt{1+\frac{4s}{Pe}}}{2/Pe}}$$

Equation 3.15

Applying inverse Laplace it is obtained the residence times distribution function

$$E(\theta) = \mathcal{L}^{-1}\{g(s)\} = \frac{\sqrt{Pe}}{2\sqrt{\pi\,\theta^3}}\, e^{-\frac{Pe}{4\theta}(1-\theta)^2}$$

Equation 3.16

Where, in this case, $\theta = \frac{t}{(1-\alpha-\beta)\,\tau}$.

The next step is the mole balance to the CSTR with the stagnant zone, starting with the CSTR balance

$$v\,C_1 + \gamma\,v\,C_2 = v\,C_O + \gamma\,v\,C_O + \alpha V\frac{dC_O}{dt}$$

Equation 3.17

Dividing by $v$

$$C_1 + \gamma\,C_2 = C_O + \gamma\,C_O + \alpha\tau\frac{dC_O}{dt}$$

Equation 3.18

$$\therefore \frac{dC_O}{dt} = \frac{(C_1 - C_O) + \gamma(C_2 - C_O)}{\alpha\tau}$$

Equation 3.19

Introducing the Euler method for numerical integration yields

$$C_{O_i} = C_{O_{i-1}} + \frac{\left(C_{1_{i-1}} - C_{O_{i-1}}\right) + \gamma(C_{2_{i-1}} - C_{O_{i-1}})}{\alpha\tau}dt$$

Equation 3.20

The balance to the stagnant zone comes

$$\gamma\,v\,C_O = \gamma\,v\,C_2 + \beta V\frac{dC_2}{dt}$$

Equation 3.21

Dividing by $v$

$$\gamma\,C_O = \gamma\,C_2 + \beta\tau\frac{dC_2}{dt}$$

Equation 3.22

$$\therefore \frac{dC_2}{dt} = \frac{\gamma(C_O - C_2)}{\beta\tau}$$

Equation 3.23

Introducing the Euler method,

$$C_{2_i} = C_{2_{i-1}} + \frac{\gamma(C_{O_{i-1}} - C_{2_{i-1}})}{\beta\tau} dt$$

Equation 3.24

The final equations used to design the model are then

PFR: $$C_1 = \frac{1}{(1-\alpha-\beta)\tau} \frac{\sqrt{Pe}}{2\sqrt{\pi\left(\frac{t}{(1-\alpha-\beta)\tau}\right)^3}} e^{-\frac{Pe}{4\left(\frac{t}{(1-\alpha-\beta)\tau}\right)}\left(1-\left(\frac{t}{(1-\alpha-\beta)\tau}\right)\right)^2}$$

Equation 3.25

CSTR: $$\frac{dC_O}{dt} = \frac{(C_1-C_O)+\gamma(C_2-C_O)}{\alpha\tau}$$

Stagnant zones: $$\frac{dC_2}{dt} = \frac{\gamma(C_O-C_2)}{\beta\tau}$$

To solve these differential equations the Simpson's one-third rule was applied and the model was built with a $dt$ of 0.064 h in a total of 64 hours. The cumulative distribution curve, F($t$), presented in Hydrodynamic characterization of the bioanode, was also obtained with Simpson's one-third rule. The term $\tau$, or hydraulic retention time (HRT) is calculated from the F($t$) curve, obtained by plotting C($t$)/$C_0$ as a function of time. On the other hand, the theoretical hydraulic retention time ($HRT_T$) is the ration between the volume of the reactor and the influent flow rate: $HRT_T = \frac{V}{v}$.

## 3.4. Control and data acquisition

### 3.4.1. Potentiostatic system

Throughout all the investigation the bioelectrochemical reactor was connected to a potentiostat. This allowed the control the potential of the working electrode (anode) at the desired value (-0.1 V). All potential values reported in this thesis are expressed with respect to the potential of standard hydrogen electrode (SHE), for convention the potential of this electrode is assigned the value of 0.000 V, at all temperatures, and for a solution that contains hydrogen ions at unit

activity in equilibrium with hydrogen gas at 1 atmosphere. The potentiostat was controlled by a software (EC-Lab®, BioLogic Science Instruments) which allowed to continuously record the electrochemical parameters, such as current and charge flowing in the system.

The integral of current $i$ (ampere) over time $t$ (seconds) (Equation 3.26) gives the value of electric charge $Q$ (Coulombs), which is proportional to the amount of electrons transferred in the system through the Faraday constant (F = 96 485 coulomb $mole^{-1}$).

$$Q = \int i \, dt$$

Equation 3.26

## 3.5. Analytical measurements

### 3.5.1. Methane and hydrogen determination

The concentration of methane produced in the MEC was analyzed by injecting 50 µL of headspace sample (from the glass chamber of each compartment), with a gas-tight syringe (Hamilton), into a gas-chromatograph Varian 3400 (Lake Forest, CA, USA), equipped with a flame ionization detector (FID) set to 260 ºC and a 2 m × 2 mm glass column packed with 60/80 mesh Carbopack B/1% SP-1000, using He as the carrier gas at a flow rate of 18 mL $min^{-1}$ and the oven temperature set at 50 ºC. As for hydrogen, its concentration was quantified in the same gas-chromatograph but with a thermal-conductivity detector (TCD) set to 200 ºC and a stainless-steel column packed with molecular sieve, using He as gas carrier at 18 mL $min^{-1}$ and the oven temperature at 180 ºC. The volume of gaseous sample injected was 500 µL, also using a gas-tight syringe. The chromatographic peaks were integrated by the internal software of the gas chromatograph, and their quantification was achieved through the calibration curve, obtained by linear regression of chromatograph peak areas measured from the analyses of standard bottle's headspace samples. Those standards were prepared in well-known volume bottles, with a defined concentration of gas ($CH_4$ or $H_2$). There were four bottles of each gas with crescent concentration expressed in percentage of volume of gas added per bottle volume.

The headspace concentrations were converted to aqueous-phase concentrations using tabulated Henry's law constants, i.e.: methane, K = 30.57 at 25 ºC; and hydrogen, K = 51.9 at 25 ºC. The calculation of the total production of biogas was taken into account both the liquid and gaseous phase concentrations.

### 3.5.2. Acetate determination

The acetate present in the influent and effluent of the MEC anodic compartment was measured by using a Dani Master GC (Milan, Italy) gas chromatograph equipped with a FID set to 200 ºC and a 2 m × 2 mm glass column packed with Carbopack as the stationary phase at 175 ºC, and using He as the carrier gas at 25 mL $min^{-1}$.

The collected liquid samples were filtered (0.22 μm porosity) and stored at -4 ºC before being analyzed. To 1 mL of unfrozen sample 100 μL of a 0.33 M concentrated solution of oxalic acid and 100 μL of a 2 g $L^{-1}$ concentrated solution of acrylic acid (functioning as internal standard) were added. If necessary, samples were diluted.

In order to determine the calibration curve, standard solutions of acetic acid (with a concentration range between 0 and 3.63 mM) were similarly prepared, from a concentrated solution of sodium acetate (3.63 mM). As acrylic acid was used as the internal standard, the calibration curve reported the ratio between the peak area of the acetic acid and that of acrylic acid as a function of acetate concentration.

The obtained chromatograms were integrated by using the computer software Clarity. The retention times were about 3 min for acetic acid and 9 min for acrylic acid.

### 3.5.3. Ammonium ion determination

The ammonium ion ($NH_4^+$) concentration present in the anodic (influent and effluent lines) and cathodic samples was assayed spectrophotometrically by the direct Nessler method – linear in the range from 0.4 to 4 mgN $L^{-1}$ (APHA 1995). The samples used for ammonium analysis were the same as those used for acetic acid analysis, but prepared according to a different procedure: to 200 μL of unfrozen sample, 5 mL of distilled water, 2 drops of Seignette salt and 100 μL of Nessler reagent were added. After at least 15 min the samples were analyzed in spectrophotometer (SHIMADZU, Spectrophotometer UV-1800) at 410 nm. The Nessler reagent consists of a solution of potassium iodomercurate which reacts with the ammonia content of the sample, originating a colored complex ($NH_3HgI_2$), according to the following reactions:

$$2(HgI_2 + KI) + 2NH_3 \rightarrow 2(NH_3HgI_2) + 2KI$$

$$2(NH_3HgI_2) \rightarrow NH_2Hg_2I_3 + NH_4I$$

Following the same procedure, ammonium chloride standards with concentrations from 0 to 75 mgN $L^{-1}$ were prepared and analyzed to determine a calibration curve which allowed the calculation of ammonium content in each sample.

### 3.5.4. Suspended solid determination

The biomass in the effluent lines (anodic and cathodic) was measured as total suspended solids (TSS) and volatile suspended solids (VSS) according to standard methods (APHA 1995), modified due to the small amount of sample available. For each analysis, 50 mL of the anode effluent line and the cathode recycle line were taken and the samples were filtered under vacuum through GF/C filters (Whatman, Cat. No. 1822-047, 47 mm of diameter), previously weighted ($P_1$). Those filters were pre-treated (at 100 ºC in oven during 24 h) and stored in a desiccator at room temperature. After sample filtration, filters were incubated again at 100 ºC for at least 4h, then transferred for 30 min into the desiccator and weighted ($P_2$). Finally, filters were treated in muffle at 550 ºC for 30 min, kept in desiccator for 30 minutes and then weighted ($P_3$). The corresponding TSS, inert suspended solids (ISS) and VSS were calculated as follows:

$$TSS(mg\ L^{-1}) = \frac{P_2 - P_1}{V}$$

Equation 3.27

$$ISS(mg\ L^{-1}) = \frac{P_3 - P_1}{V}$$

Equation 3.28

$$VSS(mg\ L^{-1}) = TSS - ISS$$

Equation 3.29

### 3.5.5. Chemical Oxygen Demand determination

The chemical oxygen demand (COD) determination was carried out by means of a COD cell test with a measuring range of 50 – 500 mgCOD $L^{-1}$ (Merck Cat. No. 1.14690.0001). This method is based on the oxidation of the sample with a hot sulfuric solution of potassium dichromate, with silver sulfate as the catalyst. The concentration of unconsumed yellow $Cr_2O_7^{2-}$ ions is then determined spectrophotometrically (SHIMADZU Spectrophotometer UV-1800) at 445 nm.

The calibration curve was obtained based on glucose standards within a 100 – 400 mgCOD $L^{-1}$ range.

### 3.5.6. Bromide anion determination

The concentration of bromide ion ($Br^-$) was assayed in the anodic effluent and in the feeding solution, by means of ion chromatography, using a Dionex ICS-1000 IC instrument, equipped with anionic AS15 column and AG14 pre-column, conductivity detector, MMS suppressor and an auto-sampler Dionex AS40 associated. The eluent composition was 4.8 mM $Na_2CO_3$ and 0.6 mM $NaHCO_3$, the eluent flow was at 1.2 mL $min^{-1}$ (in the pressure range 1800-2000 psi). All samples were diluted in 1:10 using deionized water. The calibration curve was based on potassium bromide standards within a 10 – 50 mg $L^{-1}$ range (as bromide) and the peak areas of both samples and standards were integrated by the internal software of the ion chromatograph.

### 3.5.7. Scanning electron microscopy analyses

After all the experiments, the MEC was disassembled and samples of graphite granules were collected from the anode and cathode compartments, at different locations of each compartment (near the inlet (IN) and the outlet (OUT) streams); also a piece of the internal Nafion membrane was collected. In order to perform scanning electron microscopy analysis (SEM), the samples were rinsed with phosphate buffer solution (50 mM), and immediately fixed using a solution of glutaraldehyde (50 g $L^{-1}$), for 4 hours at 4 ºC. This was removed by several washes with the buffer solution previously used. Then, the samples were immersed in osmium tetroxide solution (15 mg $L^{-1}$), for 4 hours at 4 ºC. Samples were then subjected to a serial dehydration protocol using increasing concentrations of ethanol (65, 75, 95 and 100, for 5, 15, 30, 60 min respectively for each stage with very gentle periodic agitation) and then dried completely at room temperature.

## 3.6. Calculations

Throughout the experimentation the MEC performance has been evaluated in terms of substrate removal efficiency, current generation, methane and hydrogen production, cathode capture efficiency, and energy efficiency; calculated as follows:

The acetate or COD removal efficiencies at the MEC anode were calculated as:

$$Removal\ efficiency\ (\%) = \frac{Conc_{IN} - Conc_{OUT}}{Conc_{IN}} \times 100$$

Equation 3.30

Where $Conc_{IN}$ and $Conc_{OUT}$ are the influent and effluent acetate or COD concentrations, respectively.

The cumulative electric charge, as milliequivalents ($meq_i$), that was transferred was calculated by integrating current (A) over time (s) and dividing by the Faraday constant, $meq_i = \frac{\int_0^t i\,dt}{F}$. Cumulative equivalents released from the substrate's oxidation, $meq_S$, or recovered as methane and hydrogen, $meq_{CH_4}$ and $meq_{H_2}$, were calculated from their measured amounts (mmol), considering the corresponding molar conversion factor in molar equivalents, as shown in Table 3.1.

Table 3.1 - Anodic and cathodic reactions occuring in the MEC.

| | **Anodic Oxidation Reaction** | | **Conversion factor** |
|---|---|---|---|
| Acetate | $CH_3COO^- + 4\ H_2O \rightarrow 2\ HCO_3^- + 9\ H^+ + 8\ e^-$ | | 8 eq $e^-$ / mole $CH_3COO$ |
| Water | $2\ H_2O \rightarrow O_2 + 4\ H^+ + 4\ e^-$ | | 2 eq $e^-$ / mole $H_2O$ |
| | **Cathodic Reduction Reaction** | **ΔG (kJ $mol^{-1}$)** | |
| $CO_2$ to $CH_4$ | $CH_4 + 2\ H_2O \rightarrow CO_2 + 8\ H^+ + 8\ e^-$ | -817.97 | 8 eq $e^-$ / mole $CH_4$ |
| $H^+$ to $H_2$ | $H_2 \rightarrow 2\ H^+ + 2\ e^-$ | | 2 eq $e^-$ / mole $H_2$ |

At the anode, the coulombic efficiency (CE) indicates the equivalents of the oxidized substrate recovered as current. While the experiment runned with acetate as substrate, coulombic efficiency was calculated as:

$$CE_{Ac}(\%) = \frac{\int_0^t i\,dt/F}{mol\ acetate \cdot 8} \times 100 = \frac{meq_i}{meq_{Ac}} \times 100$$

Equation 3.31

Once the substrate was changed to the complex solution, the overall substrate was measured as COD and the equivalents released from its oxidation were calculated taking into account that 1g of COD corresponds to 4/32 equivalents, considering the water oxidation reaction (reported in Table 3.1), and the molecular weight of $O_2$ (32 g $mol^{-1}$).

In this case coulombic efficiency was calculated by:

$$CE_{COD}(\%) = \frac{\int_0^t i\,dt/F}{\left(g_{COD_{in}} - g_{COD_{out}}\right) \cdot Q \cdot t \cdot \frac{4}{32\frac{gO_2}{mol}}} \times 100 = \frac{meq_i}{meq_{COD}} \times 100$$

Equation 3.32

Concerning to cathode, the coulombic efficiency represents the amount of electrons used to produce methane or hydrogen with respect to the electrons transferred in the system. This efficiency was named cathode capture efficiency (CCE) and calculated as:

$$CCE_{CH_4}(\%) = \frac{mol_{CH_4} \cdot 8}{\int_0^t i\, dt/F} \times 100 = \frac{meq_{CH_4}}{meq_i} \times 100$$

Equation 3.33

$$CCE_{H_2}(\%) = \frac{mol_{H_2} \cdot 2}{\int_0^t i\, dt/F} \times 100 = \frac{meq_{H_2}}{meq_i} \times 100$$

Equation 3.34

The MEC energy efficiency ($\eta_E$) was calculated as the energy that can be theoretically recovered from the produced methane relative to the electrical energy input to the system:

$$\eta_E(\%) = \frac{mol_{CH4} \cdot \Delta G_{CH4}}{C \cdot \Delta V} \cdot 1000 \cdot 100$$

Equation 3.35

In the numerator the energy recover (kJ) as methane is calculated, from the total amount of methane produced ($mol_{CH4}$, mol) and the molar Gibbs free energy of methane oxidation by oxygen to carbon dioxide (Table 3.1). Denominator is the electrical energy added to the system, where $C$ represents the total Coulombs, calculated from $\int_0^t i\, dt/F$, and $\Delta V$ (V) is the difference of potential between the cathode and anode of the MEC. Observing Equation 3.33, it is also possible to calculate energy efficiency from:

$$\eta_E(\%) = \frac{CCE \cdot \Delta G_{CH4}}{8 \cdot F \cdot \Delta V} \cdot 1000$$

Equation 3.36

# 4. Results

## 4.1. Microbial electrolysis cell (MEC)

This experimental work started with the bioelectrochemical reactor already running, thus operative conditions such as pH, operation temperature and flow rates were previously established. The MEC results will be divided in two major parts: Run I, when MEC worked at a controlled anode potential of -0.1 V *vs.* SHE (standard hydrogen electrode) using acetate solution as the substrate, corresponding to an applied OLR of 1.08 gCOD $L^{-1}$ $d^{-1}$; and Run II, when anode's potential was set to -0.1 V *vs.* SHE though the reactor was fed with a synthetic wastewater that corresponded to an applied OLR of 0.93 gCOD $L^{-1}$ $d^{-1}$. The variations made during both studies are as follows.

### Run I: Performance of the MEC fed with a synthetic solution containing acetate as sole carbon source (bioanode potential controlled at -0.1 V *vs.* SHE)

The first run of this research (Run I) was monitored through around 60 days, in the frame of a larger study aimed to investigate the effect of the anode potential (between +0.2 and -0.2 V *vs.* SHE) on the MEC performance. Figure 4.1 indicates the potential applied to the bioanode at each period. For the first six days of operation the system performance was studied at a bioanode potential of 0 V and for the following twenty days the potential was set to -0.2 V. The subsequent sixty days are the focus of this section. More in details, this experimentation started on day 33 of the major run, when the bioanode potential was set at -0.1 V.

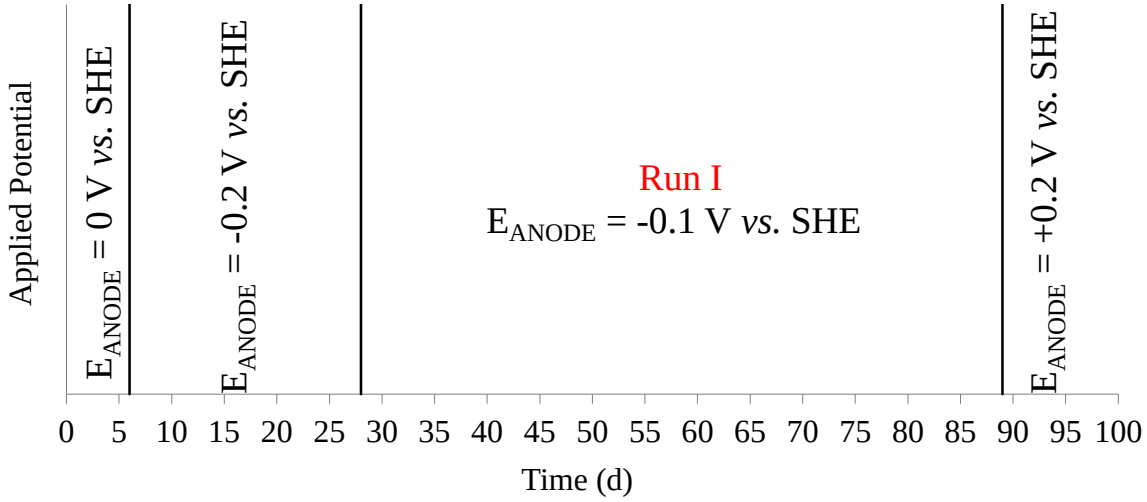


Figure 4.1 - Potential applied to the bioanode overtime. Run I of this experimentation started on day 33, when the bioanode potential was controlled at -0.1 V *vs.* SHE.

Through the entire run, the MEC bioanode was continuously fed with acetate at a fixed influent concentration of 640 mgCOD $L^{-1}$, corresponding to an applied OLR of 1.08 gCOD $L^{-1}$ $d^{-1}$. As it is reported in Figure 4.2 A, the effluent acetate concentration ranged around 88.11 ± 8.88 mgCOD $L^{-1}$ during Run I, which indicates a high acetate removal efficiency with an average value of 88.61 ± 1.96 % (Figure 4.2 B). The average biomass in the anode effluent was 58.37 ± 24.92 mg $L^{-1}$ (as VSS), resulting in an observed growth yield of around 0.10 mgCOD/mgCOD (i.e., 10 %). For this calculation a steady-state was assumed, whereby the amount of microorganisms daily withdrawn from the anode compartment corresponded to the amount of newly formed biomass.

During this phase the generated current was not constant, in fact, as shown in Figure 4.3, the current was stable for a short period and then decreased, which can be due to a decrease of the bioanode activity. Therefore, in order to better describe the performance of Run I, it was decided to divide it into four periods: the first period went from day 33 thru day 49; the second period from day 53 to day 64; the third period was from day 67 to 74; finally, the last studied period was between day 75 and day 85. For the first period the average value of current generation accounted for about 89.08 ± 0.18 mA, which decreased over time down to an average value of 43.68 ± 0.08 mA by the end of Run I, as detailed in Table 4.2. At this point, the anode potential was poised at +0.2 V (*vs.* SHE) in order to verify if current returned to the previous values, as already reported in a previous study (Villano et al. 2013).

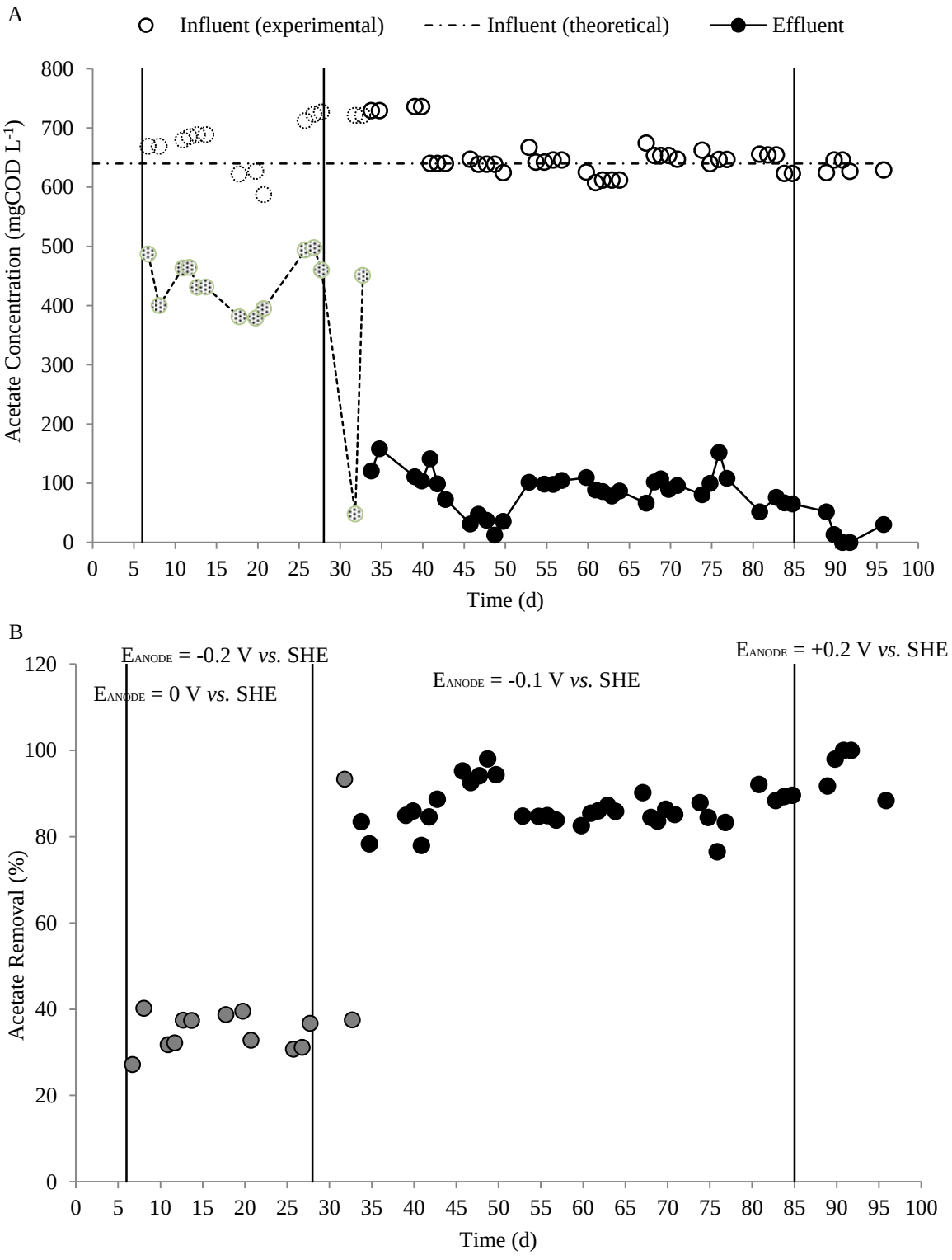


Figure 4.2 - Acetate concentration in the influent and effluent streams of MEC anode at different applied potentials (A). Percentage of acetate removal in the MEC at different applied potentials (B). The dashed line and the lighter points represent the data that is not reviewed in this study; the same succeed for the following graphics.

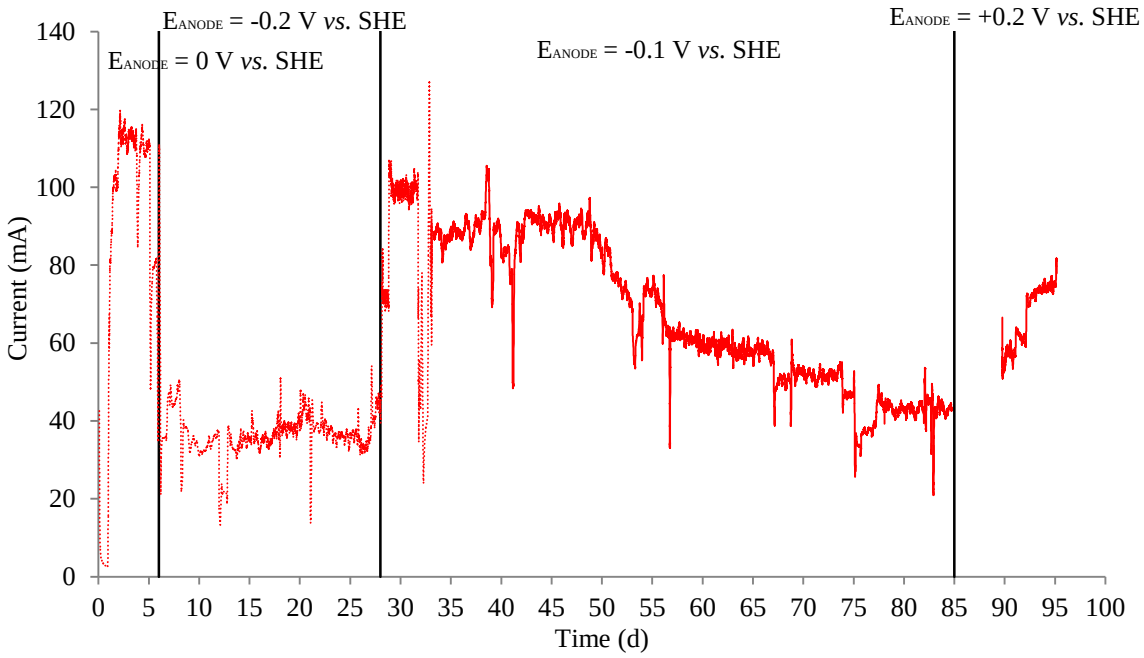


Figure 4.3 - Current generation by the activated sludge at different anode potentials. The dotted line represents the data collected on the first 33 days of the major run, and the continuous line represents the data referred to Run I.

Moreover, it was not observed a correlation between the decreasing current generation and the acetate consumption (which remained higher than 80 %), with a correspondent reduction in the coulombic efficiency (i.e. the fraction of the removed acetate converted into current, Equation 3.31) of the system (Figure 4.4). More in details, it decreased from 73.09 ± 1.09 % to 37.06 ± 1.44 %, as reported in Table 4.2.

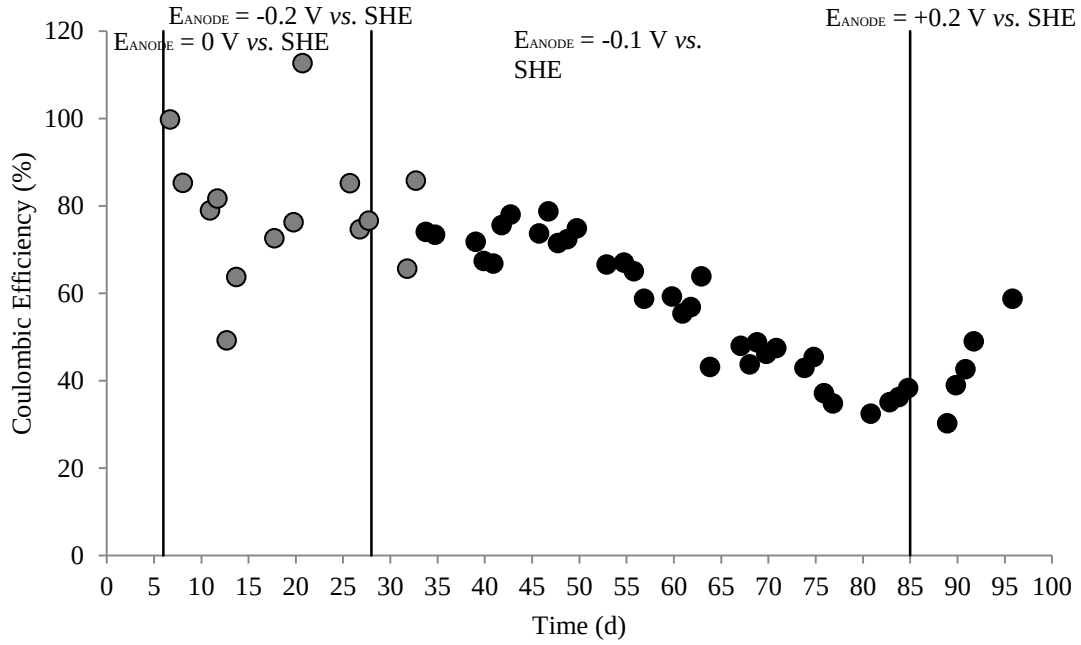


Figure 4.4 - Coulombic efficiency over time at different studied potentials.

For what concerns biogas production, Figure 4.5 A illustrates the time course of the cumulative amounts (as milliequivalents) of hydrogen and methane. The flow of electrons resulting from the microbial oxidation of acetate at the anode was mainly recovered at the cathode as methane. There was a continuous methane production, although the average production rate (Figure 4.5 B) has decreased over time during Run I from 70.65 ± 3.02 meq $d^{-1}$ to 43.46 ± 3.64 meq $d^{-1}$.

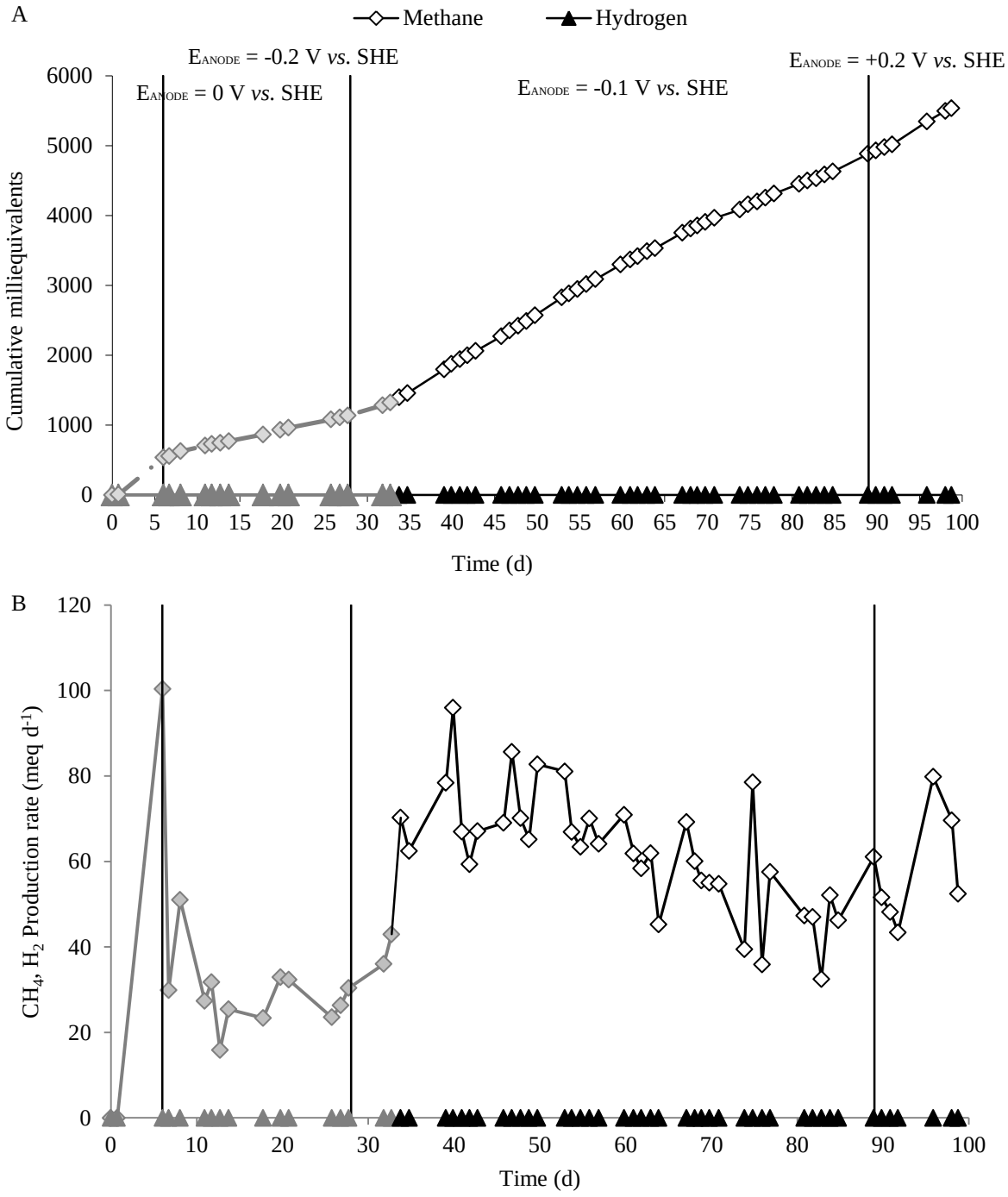


Figure 4.5 - Time course of cumulative methane and hydrogen production with the anode potential controlled at different values. In particular, Run I refers to the period that occurs from day 33 until day 85, when the anode potential was controlled at -0.1 V *vs.* SHE (A). Rate of methane and hydrogen production over time (B).

The MEC cathode capture efficiency (CCE), which represents the yield of electric current conversion into cathodic products (Equation 3.33 and Equation 3.34), is reported in Figure 4.6. As it is possible to observe the CCE remained high throughout all the experiment, though it slightly increased over time during Run I. For the first period the CCE accounted for 94.84 ± 4.22 %, in the following periods were verified values of 111.63 ± 2.81, 128 ± 6.44 and finally 124.02 ± 12.82 %. These values represented an increase of nearly 30 % during MEC's operation at the current applied potential, taking an average CCE of 114.78 ± 6.57 %.

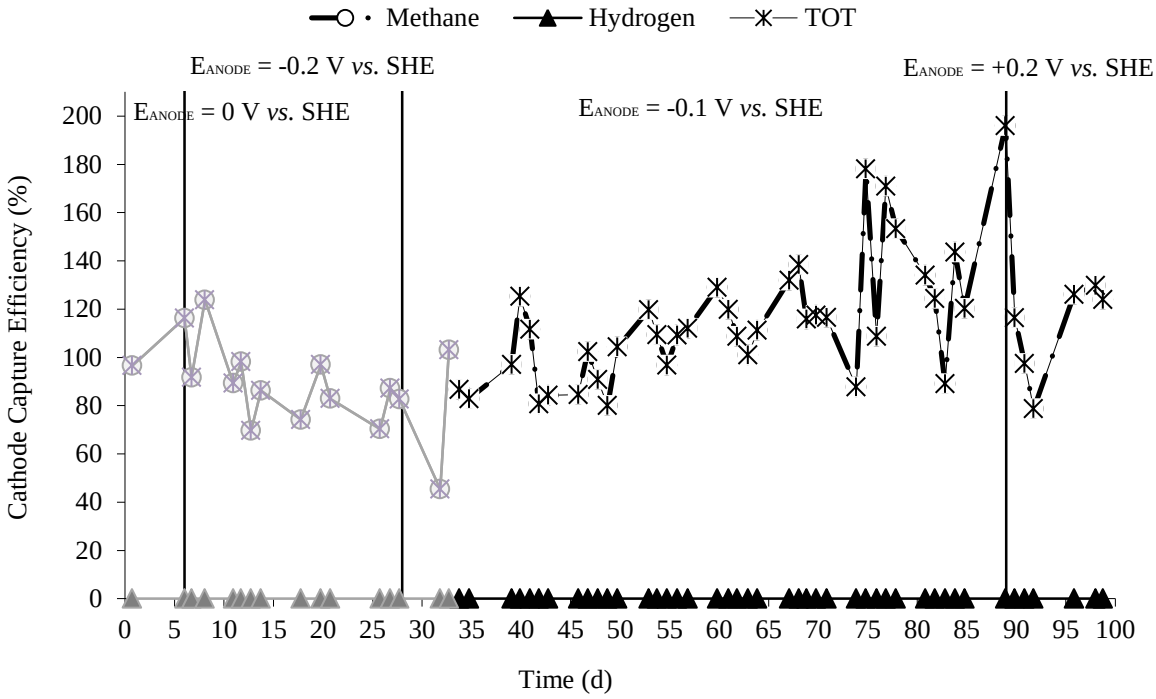


Figure 4.6 - Methane and hydrogen cathode capture efficiency during the MEC operation period.

It is worth noting that the observed high values of CCE occurred together with a decrease of current and coulombic efficiency over time. This was likely due to the fact that the membrane presented some small holes as later confirmed by the SEM analysis (see 4.3 Scanning Electron Microscopy (SEM)) which probably allowed acetate to be transferred from the anode to the cathode of the MEC, resulting in a decrease of current concomitant to high CCE.

The MEC performance was also evaluated in terms of energy efficiency, which represents the energy captured into methane gas relative to the electrical energy input. In the four periods of the experience, system's energy efficiency increased from 137.17 ± 6.27 % to 217.71 ± 13.94 %, which indicates a positive energy recovery relative to the electrical input. As indicated in Equation 3.35 and Equation 3.36, the energy input takes into account the voltage difference between the cathode and the anode of the MEC, measured under steady state conditions, for the

first three periods the ΔV was similar, and presented values as -0.743 V, -0.745 V and -0.720 V, respectively; instead for the last period the ΔV of the system accounted for -0.660 V, thus resulting in a higher energy efficiency.

Figure 4.7 demonstrates the time course of ammonium nitrogen concentration in both anode influent and effluent, as well as in the cathode compartment. The average value of the anode influent concentration was 42.14 ± 0.58 mgN-$NH_4^+$ $L^{-1}$, whereas the average value of the effluent concentration was 30.73 ± 0.91 mgN-$NH_4^+$ $L^{-1}$, corresponding to a removal efficiency of 27.8 %. On the other hand, the average ammonium concentration in the cathode compartment was quite high (261.81 ± 6.22 mgN-$NH_4^+$ $L^{-1}$), indicating that there was a preferential transport of the ammonium ion across the membrane contrary to the concentration gradient.

There are two possible mechanisms that explain the ammonium removal in the anode: assimilation into newly formed microbial cells and migration to the cathode through the proton exchange membrane to preserve the charge balance in the system (nitrification of ammonium ion into nitrite or nitrate was not considered because it had not been observed even at higher anode potential). For the microbial growth mechanism, it was estimated from the measured concentration of VSS in the anode effluent (31 ± 3 mg $L^{-1}$), the assumed nitrogen on VSS content (12.4 %, from the theoretical biomass composition of $C_5H_7O_2N$ (Villano et al. 2013)), and the effective liquid volume (1.367 L $d^{-1}$) daily removed from the anode compartment. Regarding the ions transport between both compartments, for each mole of electron that is transferred from the anode to the cathode, a mole of positive charge should migrate from the anolyte to the catholyte to conserve electroneutrality (Cord-Ruwisch et al. 2011). This contribution was estimated from the average ammonium concentration in the cathode compartment and the liquid volume (0.073 L $d^{-1}$) daily removed from the cathode compartment in order to counterbalance the liquid phase diffusing from the anode (Cord-Ruwisch et al. 2011; Kuntke et al. 2011). The steady-state nitrogen mass balance for the MEC is summarized in Table 4.1.

Table 4.1 - Steady-state nitrogen mass balance of the MEC.

| **Parameter** | **INPUT (mgN $d^{-1}$)** | **OUTPUT (mgN $d^{-1}$)** |
|---|---|---|
| $N_{Anode,\ in}$ | 60.68 | |
| $N_{Anode,\ out}$ | | |
| Soluble | | 42.00 |
| Suspended Solids | | 5.25 |
| $N_{Anode \rightarrow Cathode}$ | | 19.17 |
| **TOTAL** | **60.68** | **66.42** |

As shown in Table 4.1, the performed mass balance allowed to recover around 109.5 % of the influent nitrogen indicating that the main mechanisms involved in ammonium removal were identified.

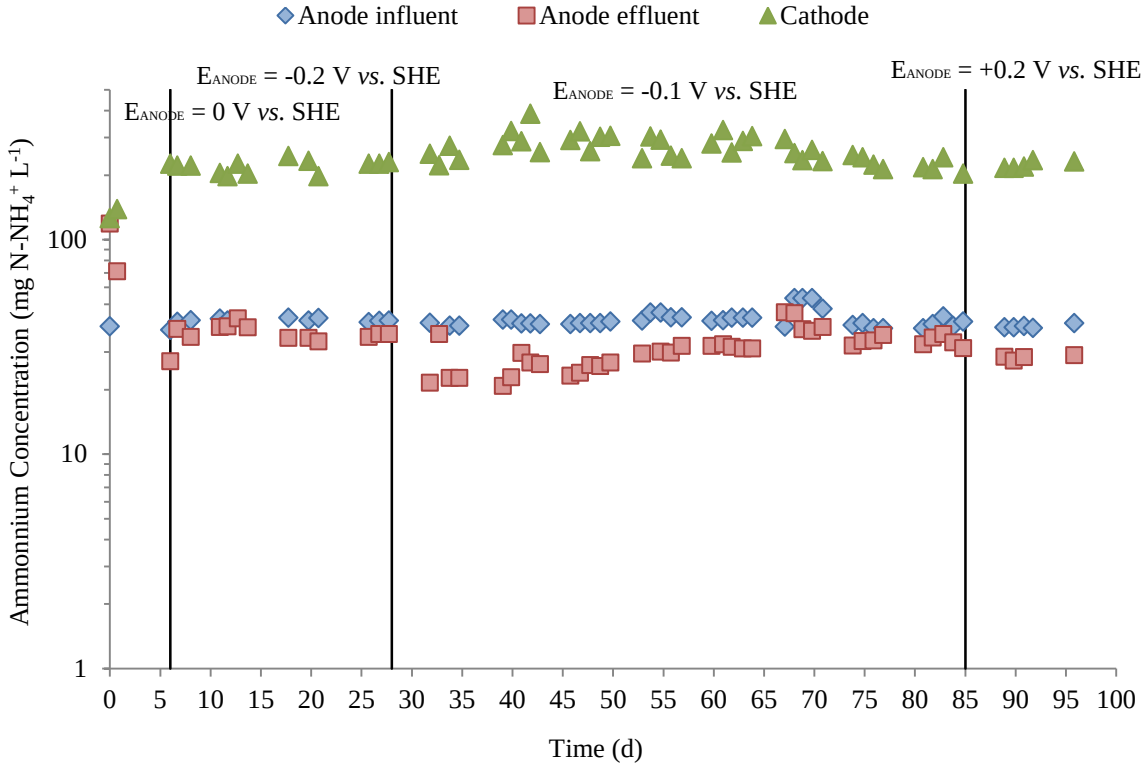


Figure 4.7 - Measured ammonium nitrogen concentration at the cathode and in both influent and effluent anode streams during the MEC operation period.

### Run II: Performance of the MEC fed with a synthetic solution containing soluble organic compounds other than acetate (bioanode potential controlled at -0.1 V *vs.* SHE)

Run II takes place after cleaning all system's tubing, changing the electrodes and performing a tracer experiment to study the fluid dynamic conditions of the reactor. The experiment starts with an applied potential of +0.2 V *vs.* SHE, while the reactor was fed with the acetate solution. As shown in Figure 4.8, the generated current immediately increased and stabilized at around 80 mA.

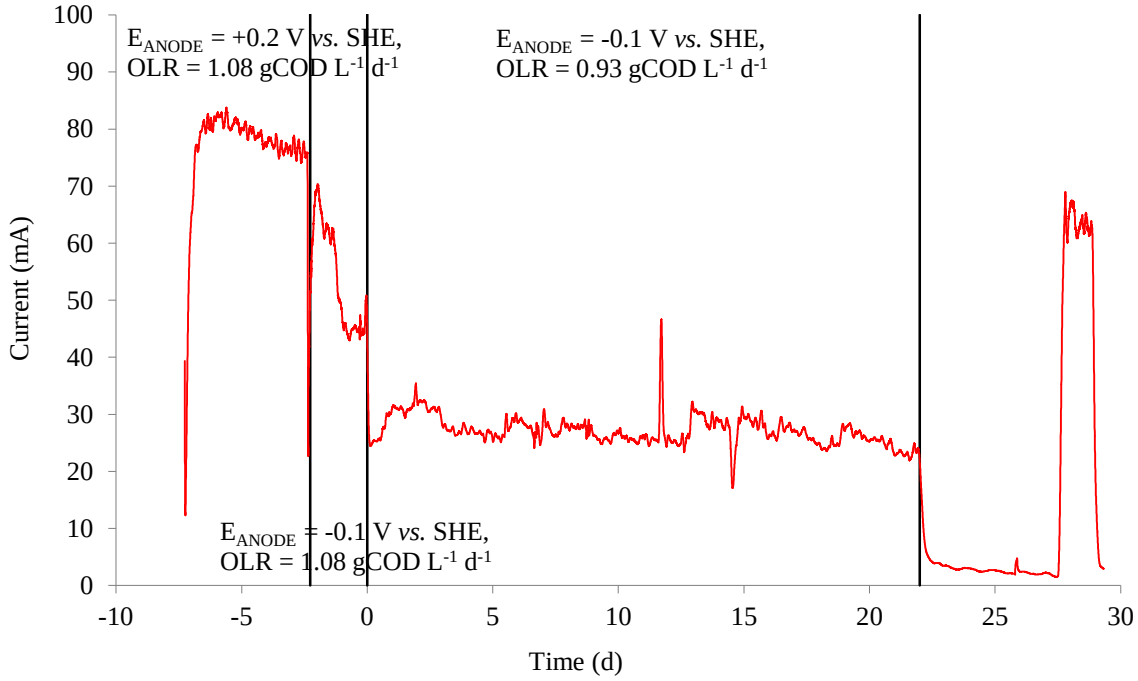


Figure 4.8 - Current generation by the activated sludge at different anode potentials and OLR, before and during Run II.

The anode potential was then decreased to -0.1 V *vs.* SHE during continuous operation, and current generation decreased because of the less oxidizing value of the anode potential and in two days the reactor performance was similar to the previously described for the end of Run I (i.e. fourth sub period of Run I). Then, the feeding solution was replaced by a synthetic solution containing soluble organic compounds other than acetate. The applied organic load rate was 0.93 gCOD $L^{-1}$ $d^{-1}$. Under these conditions the generated current had an average value of 27.13 ± 0.02 mA for the period of the experimentation, which lasted 22 days. The results obtained for substrate removal as well as reactor efficiencies are only shown for Run II time extent, i.e. from day 0 until day 22.

Concerning the substrate consumption, in this run it was studied in terms of only acetate concentration and total COD concentration though in this case it only starts on the twelfth day of operation. All the results dependent on the total COD concentration have this lack on the first twelve days due to experimental errors on the analysis. Figure 4.9 A shows the acetate concentration of both the influent and the effluent streams, which accounted for 85.23 ± 6.05 and 12.71 ± 1.67 mgCOD $L^{-1}$, respectively.

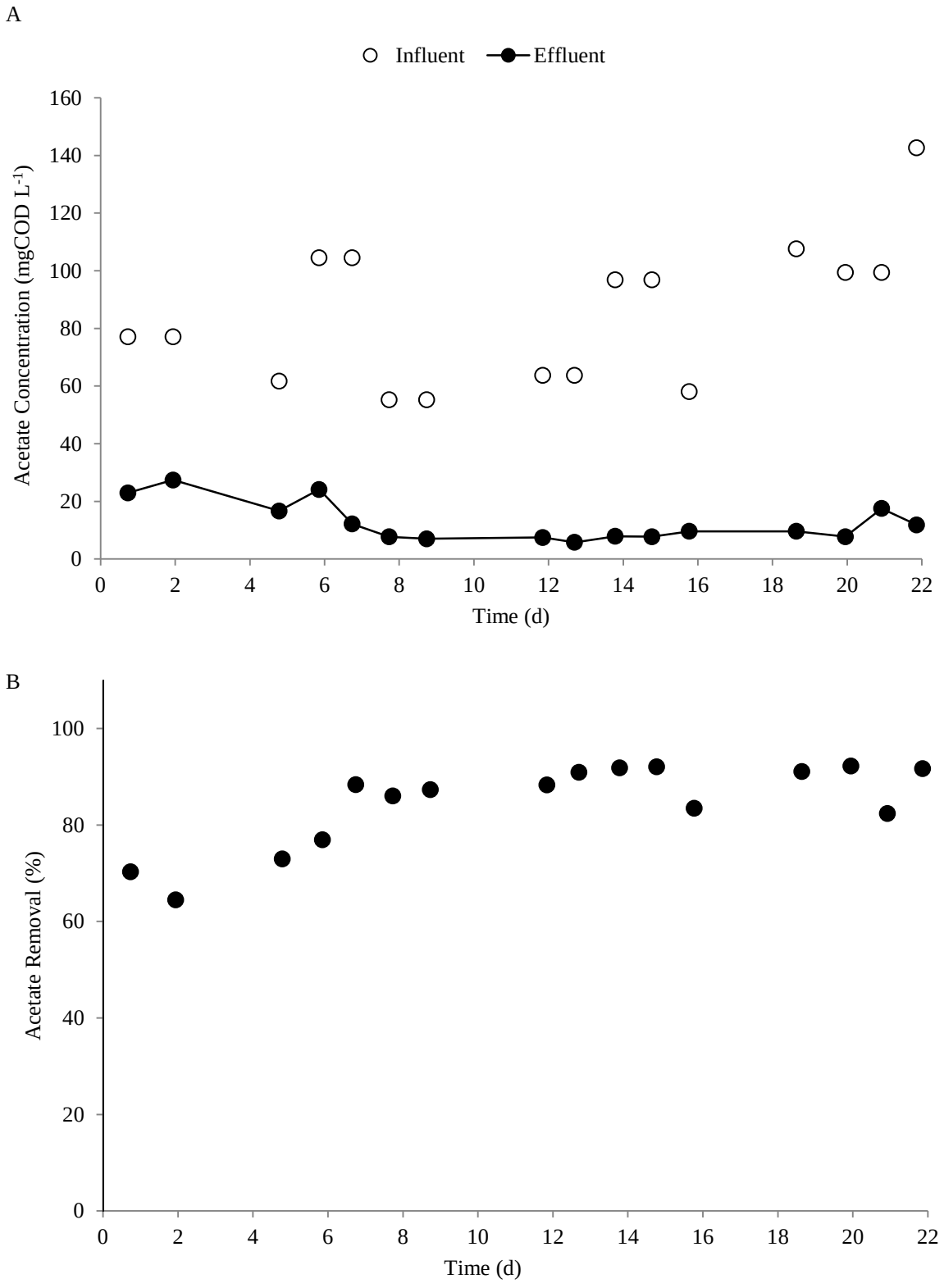


Figure 4.9 - Acetate concentration in the influent and effluent streams of the MEC anode during Run II (A). Percentage of acetate removal in the reactor during Run 2 (B).

This resulted in a high acetate removal efficiency with an average value of 84.38 ± 2.12 % (Figure 4.9 B). Regarding to total COD concentration in both streams (Figure 4.10 A), the

influent and effluent concentrations ranged around 380.70 ± 15.77 and 139.18 ± 8.65 mgCOD $L^{-1}$, respectively; resulting in an average substrate removal of 63.19 ± 2.91 % (Figure 4.10 B).

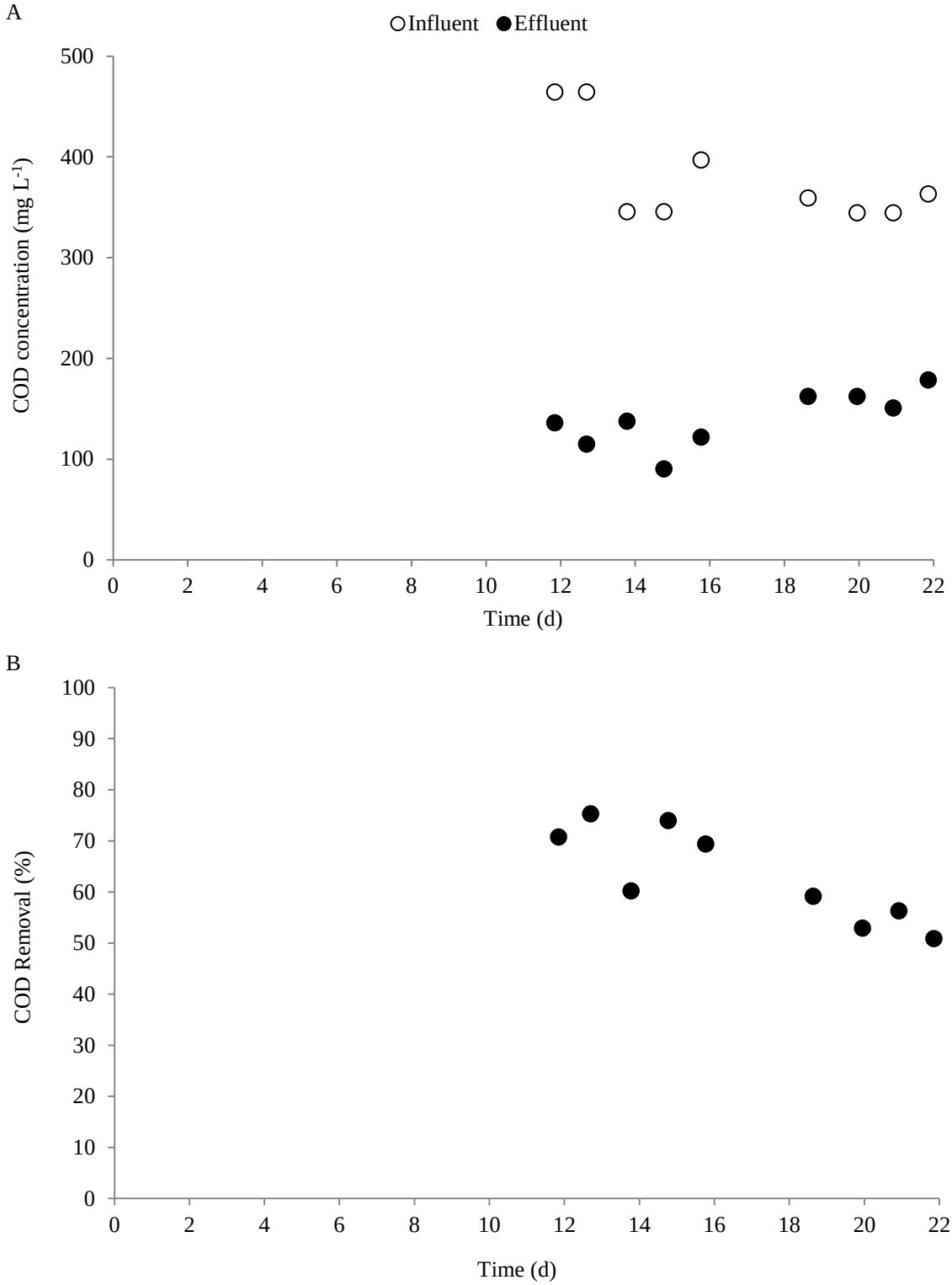


Figure 4.10 - COD concentration in the influent and effluent streams of the MEC anode during Run II (A). Percentage of COD removal in the reactor during Run II (B).

The reactor performed at an average coulombic efficiency of 57.01 ± 4.54 %, based on the COD depletion and electric current. The daily coulombic efficiency through operation time is specified in Figure 4.11. If coulombic efficiency had been calculated on acetate removal only, an average value of 216.11 ± 21.19 %, with values as high as 348 %, would have been obtained. This very high value clearly indicates that current was generated also by the oxidation of organic substrates other than acetate.

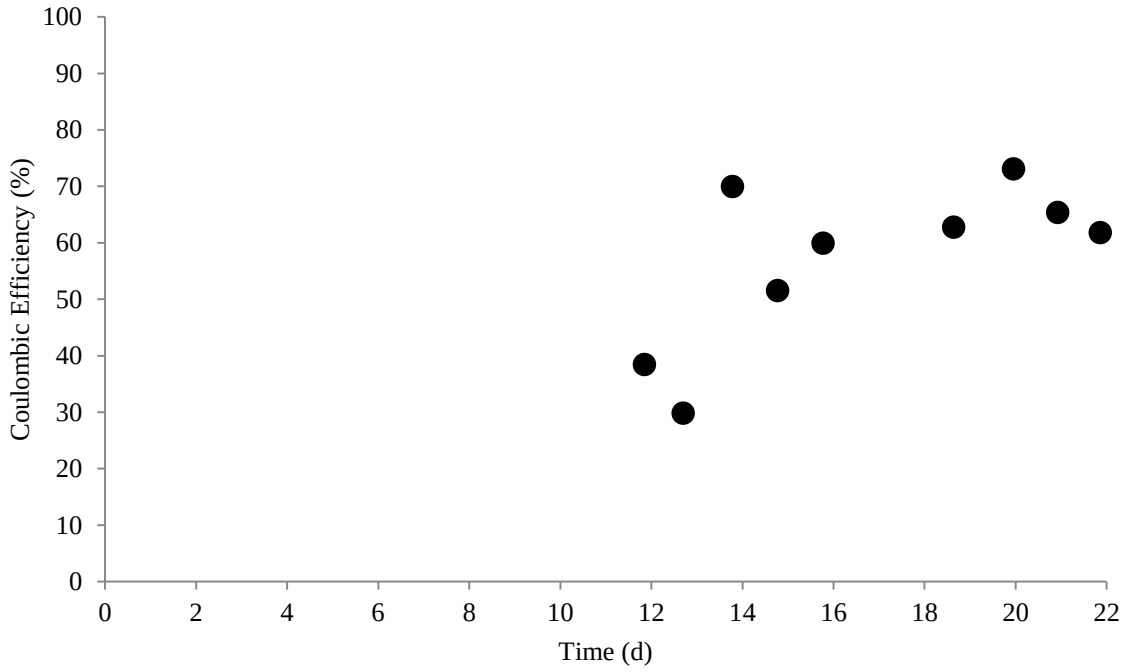


Figure 4.11 - Time course of anode's coulombic efficiency in the MEC, referred to the total COD depletion.

The next figures are about biogas production. As previously described for Run I, methane was produced continuously during the MEC operation, although in the course of Run II a decrease in the production rate was observed, likely due to the change of the substrate composition. However, that is in line with the lower production of current. Figure 4.12 A shows the cumulative amounts of hydrogen and methane (as milliequivalents) produced during the MEC operation. Methane production rate is reported in Figure 4.12 B, and accounted for an average value of 17.92 ± 1.31 meq $d^{-1}$, whereas hydrogen production was almost negligible.

The CCE is a key parameter to evaluate the performance of a methane-producing MEC, and for Run II on average 90.75 ± 5.51 % of the electric current was recovered as methane (Figure 4.13). As for the energy efficiency, it accounted for 169.76 ± 10.89 %. Since the energy input takes into account the voltage difference between the cathode and the anode, this high energy

efficiency resulted from the fact that the cathode potential stabilized at -0.67 V, resulting in a ΔV of -0.57 V.

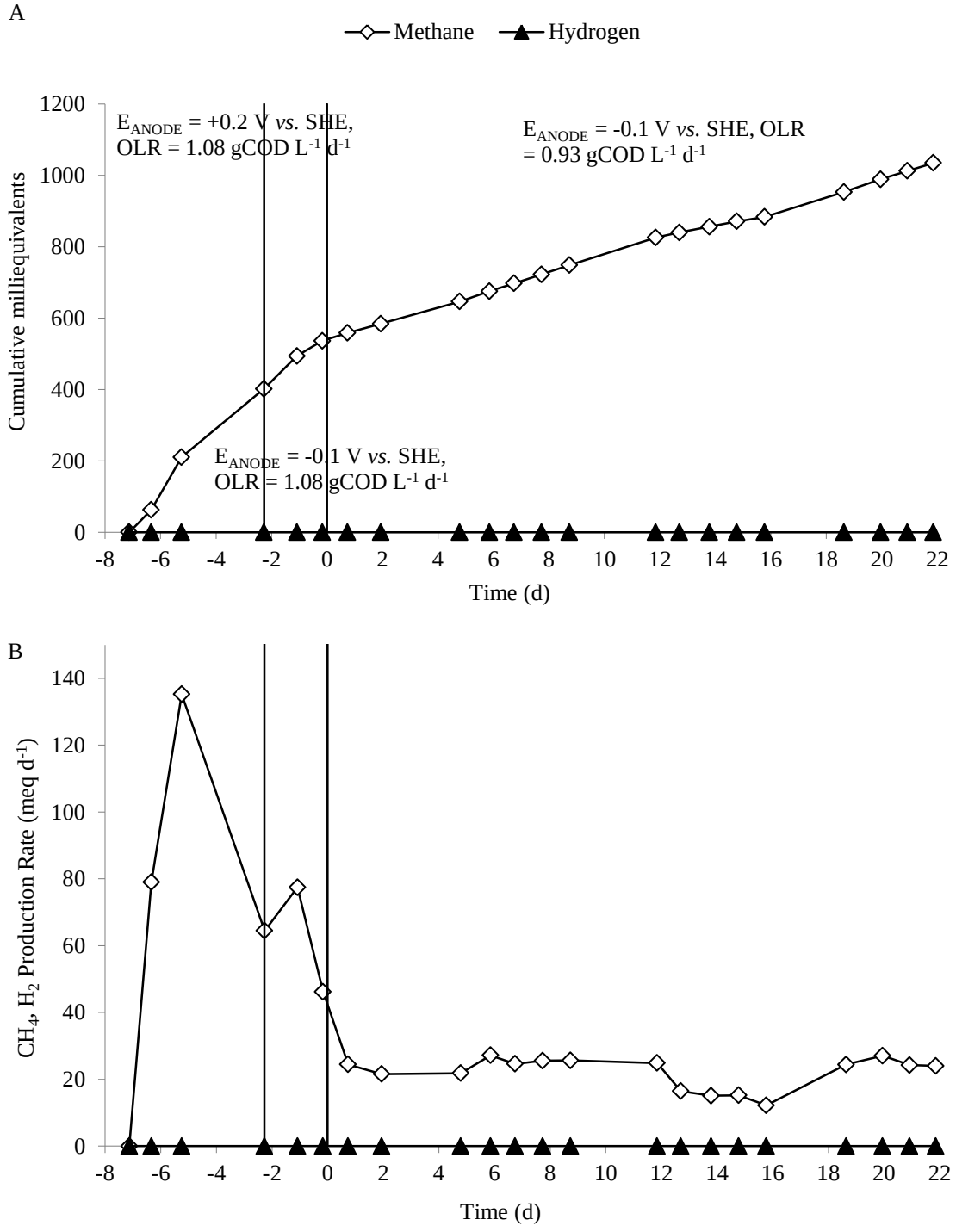


Figure 4.12 - Time course of the cumulative methane and hydrogen production throughout Run II (A). Rate of methane and hydrogen production over time (B).

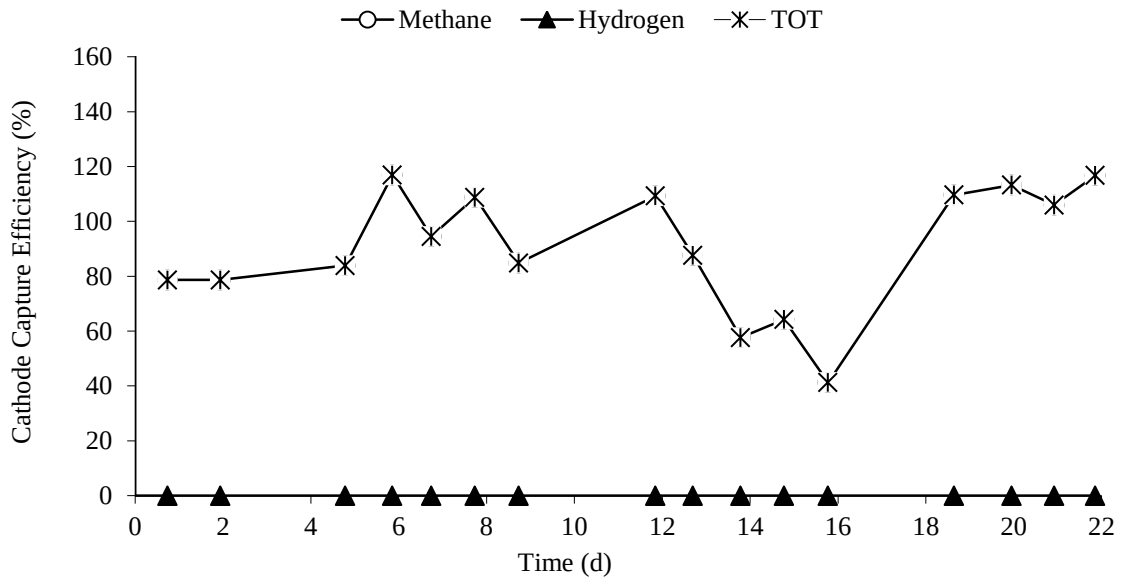


Figure 4.13 - MEC cathode capture efficiency during the Run II.

Figure 4.14 reports the ammonium nitrogen concentration in both the anode influent and effluent, as well as in the cathode compartment of the MEC. The average value of the anode influent concentration was 70.26 ± 1.15 mgN-$NH_4^+$ $L^{-1}$, whereas the average value of effluent concentration was 57.28 ± 1.85 mgN-$NH_4^+$ $L^{-1}$. On the other hand, an average concentration of 252.56 ± 9.89 mgN-$NH_4^+$ $L^{-1}$ was measured in the cathode compartment. As previously described for in Run I, the very high concentration of ammonium at the MEC cathode clearly suggests a preferential transport of the ammonium ion through the membrane against the concentration gradient. A summary of results from Runs I and II is reported in Table 4.2.

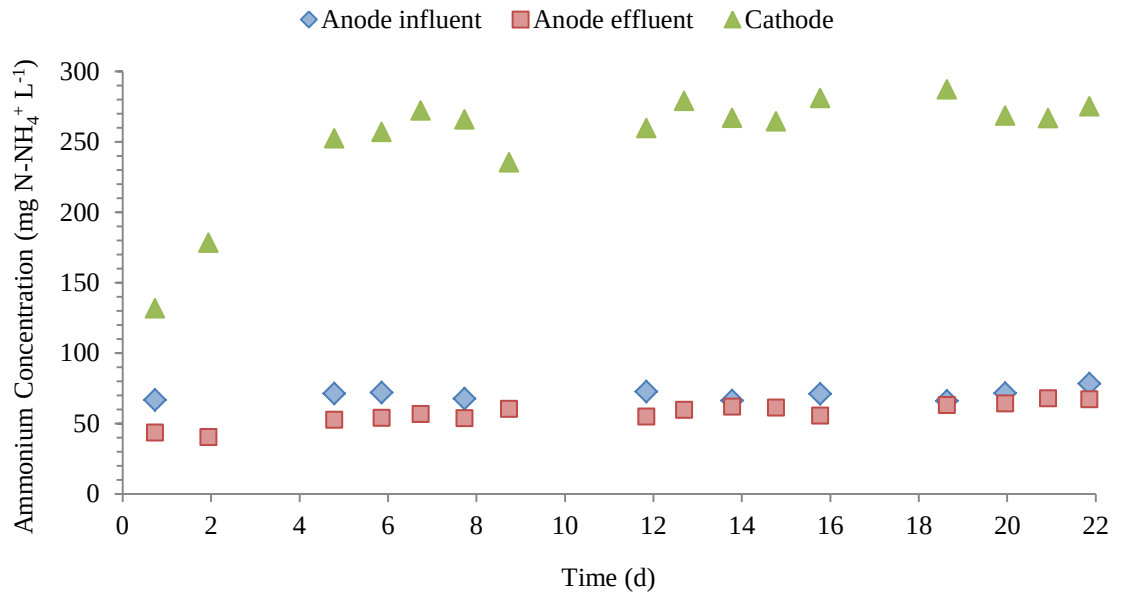


Figure 4.14 - Ammonium nitrogen concentration at the anode (influent and effluent streams) and cathode chamber of the MEC, throughout Run II.

Table 4.2 - Summary of the main parameters of the MEC operation throughout Run I and Run II.

| **Period** | **15/02/2012 to 02/03/2012** | **09/03/2012 to 18/03/2012** | **21/03/2012 to 26/03/2012** | **29/03/2012 to 06/04/2012** | **24/05/2012 to 14/06/2012** |
|---|---|---|---|---|---|
| **$E_{ANODE,\ measured}$ VS SHE (V)** | -0.1 | | | | |
| **OLR (mgCOD $L^{-1}$ $d^{-1}$)** | 1.08 | | | | 0.93 |
| **i (mA)** | 89.08 ± 0.18 | 59.69 ± 0.09 | 51.91 ± 0.09 | 43.68 ± 0.08 | 27.13 ± 0.02 |
| **Acetate removal efficiency (%)** | 88.61 ± 1.96 | 85.01 ± 0.42 | 86.24 ± 0.91 | 86.22 ± 1.84 | 84.38 ± 2.12 / COD 63.19 ± 2.91 |
| **CE (%)** | 73.09 ± 1.09 | 59.53 ± 2.36 | 46.18 ± 0.89 | 37.06 ± 1.44 | 57.01 ± 4.54 (on COD basis) |
| **$r_{CH4}$ (meq $d^{-1}$)** | 70.65 ± 3.02 | 59.17 ± 3.15 | 48.60 ± 2.90 | 43.46 ± 3.64 | 17.92 ± 1.31 |
| **$r_{CH4}$ (L $L^{-1}$ $d^{-1}$)** | 0.251 ± 0.0107 | 0.210 ± 0.0112 | 0.162 ± 0.0098 | 0.190 ± 0.0154 | 0.0637 ± 0.00467 |
| **$CCE_{CH4}$ (%)** | 94.84 ± 4.22 | 111.63 ± 2.81 | 128.62 ± 6.44 | 124.02 ± 12.82 | 90.75 ± 5.51 |
| **ηE (%)** | 137.17 ± 6.27 | 158.90 ± 4.24 | 173.98 ± 10.60 | 217.71 ± 13.94 | 169.76 ± 10.89 |

## 4.2. Hydrodynamic characterization of the bioanode

Throughout this study, a tracer experiment was carried out in order to characterize the hydrodynamic behavior of the bioanode, at two different moments. For this test, an inert tracer (KBr) was added to the feed solution and was introduced in the bioanode in a step-input mode. These experiments were performed at the end of each Run, in order to verify the occurrence of changes in the MEC fluidynamic.

Figure 4.15 shows the results of the first tracer test, performed at the end of Run I (i.e. bioanode potential set as -0.1V *vs.* SHE and acetate as carbon source), in terms of F(t) function. From this function, an actual hydraulic retention time (HRT) of 11.10 h has been calculated (as explained in 3.3. Tracer experiment). From the ratio of the actual and theoretical HRT (respectively based on void volume of the granular bed and the void volume of the empty chamber) an actual porosity of 0.67 was calculated (see Table 5.1). As an initial lag phase of 2.5 h was observed, and neither an ideal continuous-stirred tank reactor (CSTR) nor a plug-flow reactor (PFR) fit the experimental data, different combinations of these ideal reactors were tested. Three models were proposed: 1) a combination of a PFR and a CSTR in series; 2) a combination of a PFR and a CSTR in series with stagnant zones, and 3) a combination of a PFR and a CSTR with bypassing. The results for the three models were closely similar, though the variance analysis indicted the best model was the combination of a PFR and a CSTR with stagnant zones. The theoretical and experimental curves are presented in Figure 4.15, and the estimated model parameters in Table 4.3.

Table 4.3 - Parameters estimated for the theoretical model adjusted to the first tracer experiment.

| **Parameters** | |
|---|---|
| HRT (h) | 11.1 |
| Pe | 5 |
| α | 0.3 |
| β | 0.4 |
| γ | 0.2 |

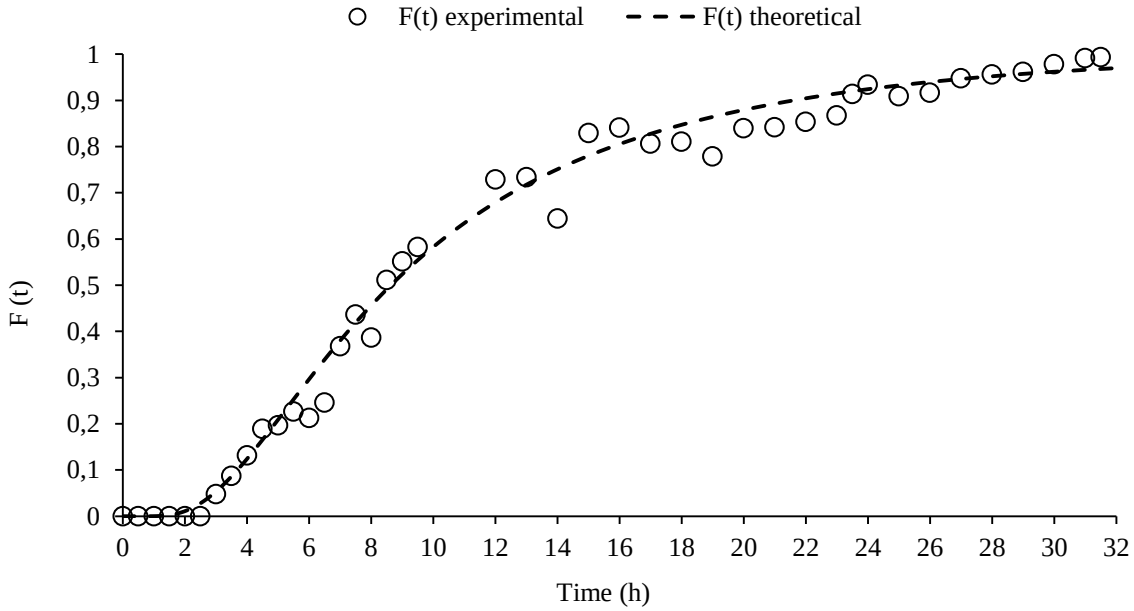


Figure 4.15 - Hydrodynamic response of the bioanode to tracer step-input as F(t) function at the end of Run I. The dashed curve represents the F(t) theoretical curve of the proposed combination of ideal reactors.

The second tracer experiment was carried out at the end of Run II (i.e. bioanode set at -0.1 V *vs.* SHE and a synthetic feeding with organic compounds other than acetate). As written in 3.3 Tracer experiment, the feed solution for this assay consisted of the usual acetate-containing medium with the tracer added, in order to study the hydrodynamic response of the bioanode along with current generation. Figure 4.16 shows the results of the tracer test in terms of F(t) function and normalized electric current (i.e. $i(t)/i_{Max}$). It can be seen that the trend of both curves is similar, though a significant lag-phase of 4 h, in the tracer response exists. The lack of a lag phase for current generation was likely due to the particular arrangement of the reactor where the liquid flow is tangential to the membrane. Hence, while the tracer and the acetate are flowing from the influent to the effluent port, acetate is immediately consumed and converted into current by the electro-active microorganisms. For this tracer experiment, the above mentioned models were also tested to interpret the hydrodynamic behavior of the reactor. In this case was considered an actual HRT of 10.42 h (corresponding to a porosity of 0.73, Table 5.1). Once again, the more adjustable model, was the combination of a PFR and a CSTR with stagnant zones. In Table 4.4 are the parameters chosen to obtain the closest possible agreement between the model and the experiment.

Table 4.4 - Parameters estimated for the theoretical model adjusted to the second tracer experiment.

| **Parameters** | |
|---|---|
| HRT (h) | 10.42 |
| Pe | 20 |
| α | 0.1 |
| β | 0.25 |
| γ | 0.08 |

The nonexistence of experimental points between 10 and 23 hours of experience is due to an experimental error that caused the rupture of Nafion membrane present in the reactor, and consequently forced the cessation of reactor's operation.

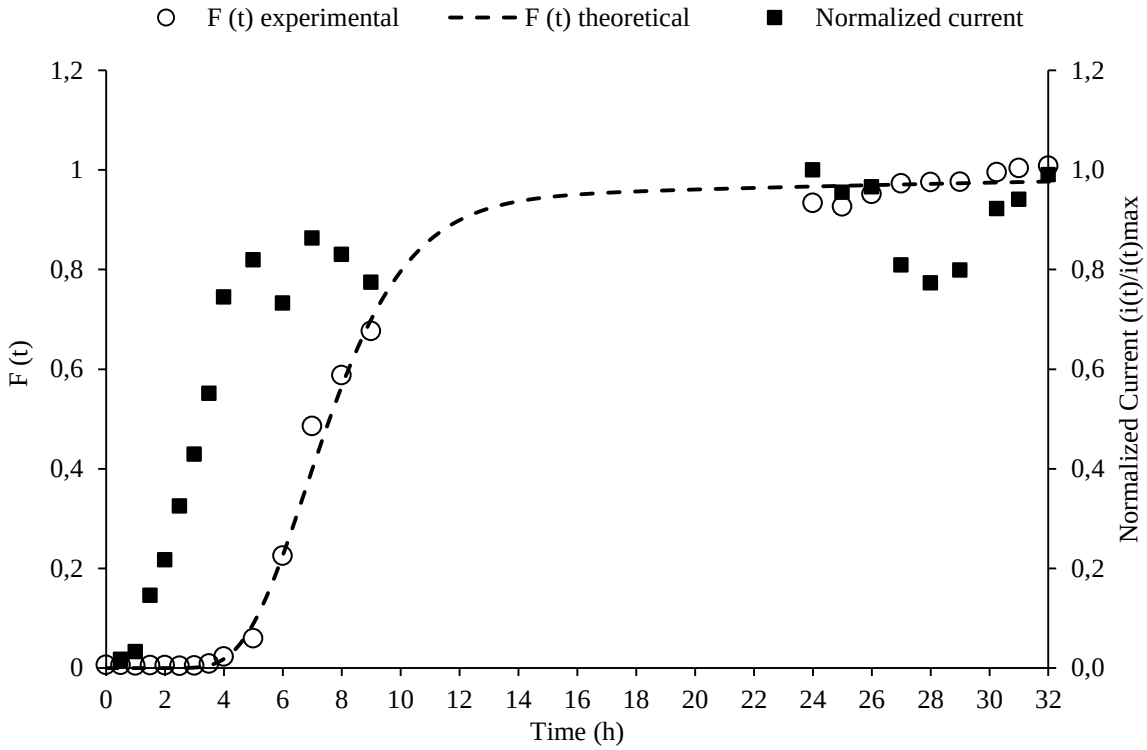


Figure 4.16 - Hydrodynamic response of the bioanode to tracer step-input as F(t) function and normalized current generation after Run II. The dashed curve represents the F(t) theoretical curve of the proposed combination of ideal reactors.

### 4.3. Scanning Electron Microscopy (SEM)

After all the experiments, the MEC was disassembled and samples of graphite granules were collected from the anode and cathode compartments, at different locations of each compartment (near the inlet (IN) and the outlet (OUT) streams); also a piece of the MEC membrane was collected. New graphite granules (i.e., not used in the MEC) were also analyzed (Figure 4.17 A) at the SEM and compared with the results obtained from the MEC graphite granules. As shown in Figure 4.17, the SEM analysis of granules from anode and cathode, as well as the membrane, showed the presence of microorganisms and, particularly, a well-developed biofilm appeared on granules from the cathode compartment (Figure 4.17 C). More in details, in Figure 4.17 B, from anode IN micrographs, it is evident a high cellular density though the bacterial morphology cannot be distinguished. However, it is visible that the biofilm density is not sufficient to cover all the cavities and the biofilm is not continuous. It is also noticeable that the voids in the used graphite are wider than those in the new graphite. On the other hand, the cathode biofilm was composed of cells with uniform morphology, as shown in Figure 4.17 C, with dominant spherical Cocci type bacteria forming the biofilm. The bacteria growing on the Nafion membrane, Figure 4.17 D, showed a morphological heterogeneity that indicates it belongs to the anodic side of the used membrane. Additionally it is possible to observe the membrane has some micrometric breaks, as indicated by the black parts seen in the figure.

Graphite granules samples taken from the outlet stream location of the reactor are shown in Figure 4.18. In the anode sample (Figure 4.18 A) the configuration observed is similar to the one observed in the samples taken in correspondence to the anode inlet, however a small colony of spherical Cocci can be seen forming on the surface of the biofilm in places with lower cellular density. Regarding the cathode sample it is perceptible a significant cellular density, and the bacterial morphology seems to be uniform, as it was in the samples collected near the influent stream of the cathode.

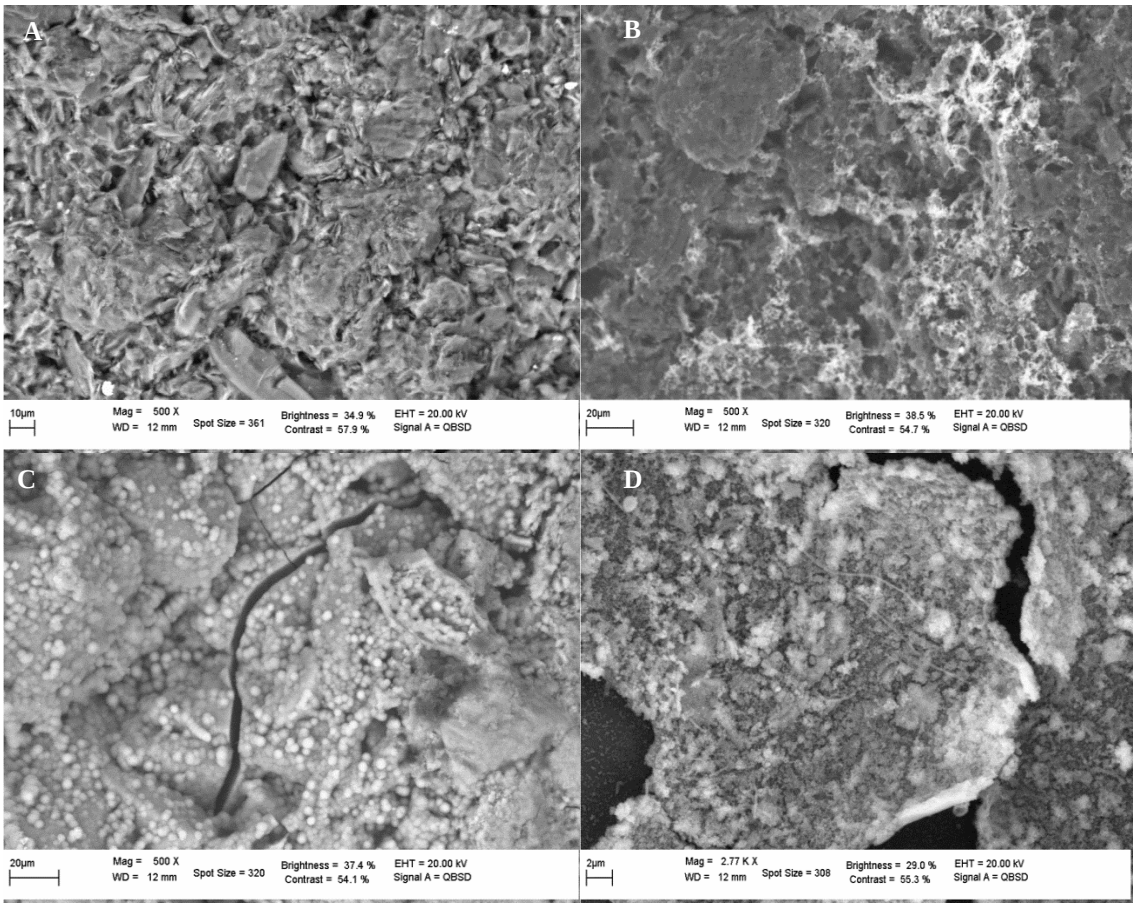


Figure 4.17 - Scanning electron micrographs, near the inlet stream of the MEC: (A) unused graphite granule, (B) bacteria growing on a bioanode graphite granule, (C) bacteria growing on a biocathode graphite granule and (D) the anodic side of Nafion membrane.

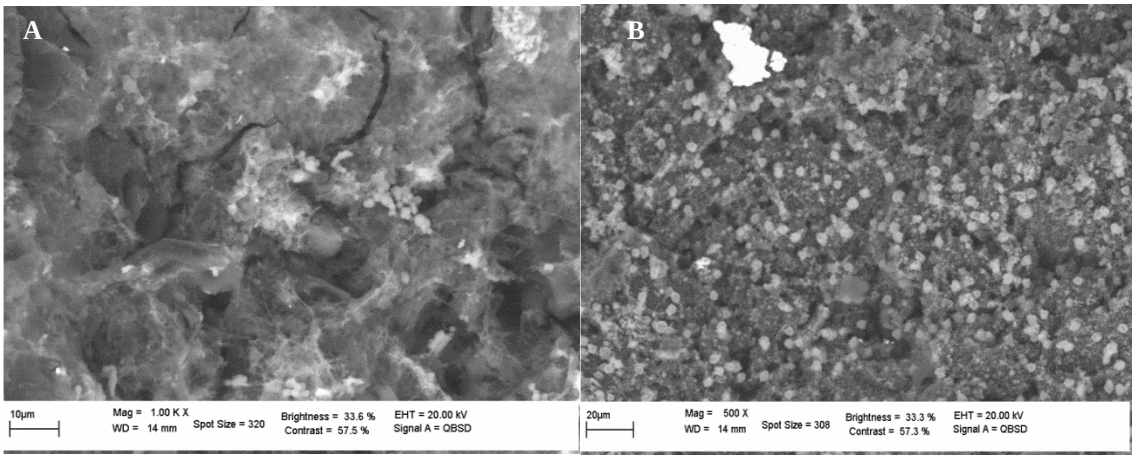


Figure 4.18 - SEM images of graphite granules taken near the outlet of the MEC: (A) anode and (B) cathode.

# 5. Discussion

## 5.1. Effect of the anode potential on the MEC performance

The results obtained in Run I, along with data acquired in previous studies, permitted to evaluate the MEC performance when submitted to different applied potentials. The most investigated operating conditions were with an applied anode potential of +0.2, -0.1 and -0.2 V *vs.* SHE; other set potentials, namely 0 and -0.15 V *vs.* SHE, were maintained for short intervals of time, therefore not allowing for the achievement of enough information to ensure its complete characterization. All experiments were operated with the same organic load rate, 1.08 gCOD $L^{-1}$ $d^{-1}$, and the other operating conditions as in Run I. In this chapter the first period of Run I was considered, as the following periods were likely biased by some malfunctioning and inappropriate performance.

An overview of the effect of the anode potential on the MEC performance is shown in Figure 5.1. The anodic substrate (acetate) removal efficiency slightly decreases when a change on the applied potential from +0.2 to -0.1 V occurs; on the other hand a sharp decrease at -0.2 V is observed. The same occurs to electric current generation; when the electrode's potential range was from +0.2 to 0 V, the average current was around 110 ± 1 mA. On the other hand, at less oxidizing values of the anode potential the current undertakes a severe decrease, achieving values as 89.08 ± 0.18, 72.36 ± 0.26 and 36.98 ± 0.05 mA at potentials of -0.1, -0.15 and -0.2 V, respectively. The close correlation between current and acetate consumption clearly indicates the ability of the inoculated sludge to use the graphite anode as terminal electron acceptor for the electrochemical substrate oxidation.

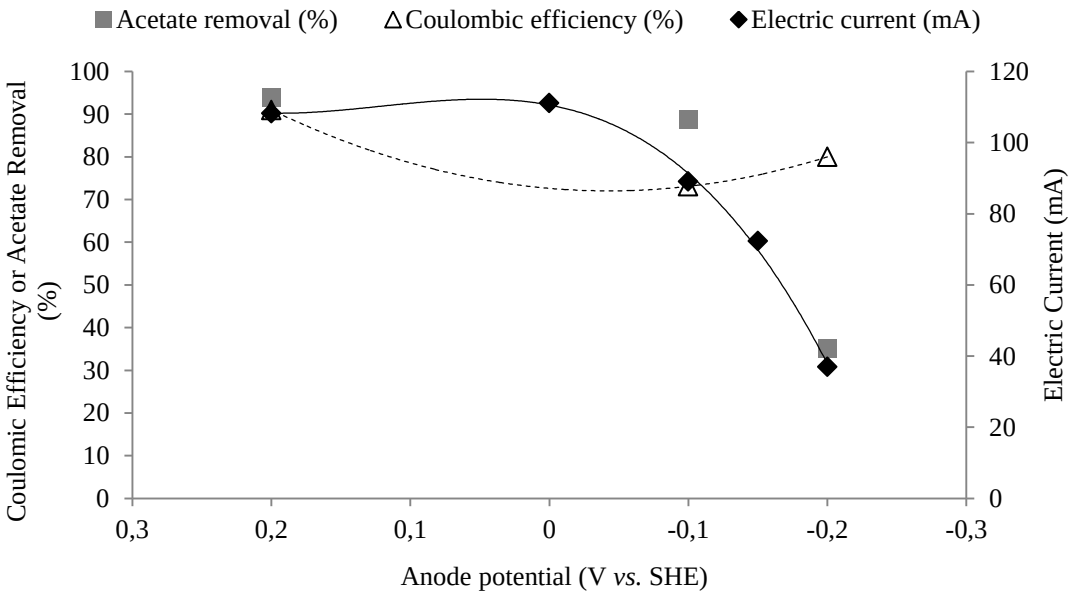


Figure 5.1 - Performance of the MEC as a function of the set anode potential in terms of: generated electric current, acetate removal efficiency, and coulombic efficiency.

When acetate is used as substrate, methanogens and electrogens can compete for the available substrate. Electrogens use the substrate to produce electrons while methanogens use the substrate to produce methane. This competition is expressed in the coulombic efficiency (CE) (Sleutels et al. 2011). In this study, since the CE remains high in the whole potential range (73.09 ± 1.09 %), it can be assumed that methanogens were not present at the MEC anode. Nonetheless at the most negative applied potential both current and substrate removal are low, which is in line with other literature studies (Wei et al. 2010), that indicates that the biocatalytic activity is affected by anode potential. Hence, these results show that lowering the applied potential has a negative effect on the acetate removal rate whereas the coulombic efficiency is rather intensive.

As current follows the trend of acetate removal in the considered potential range, so does the rate of methane production at the cathode, as it can be observed in Figure 5.2. The explanation for the lower methane production is likely due to the more negative anode potential and consequently the lower current output. Similar to the anodic CE, the cathodic capture efficiency (CCE) is also less dependent from the applied potential than the rate of the respective methane production.

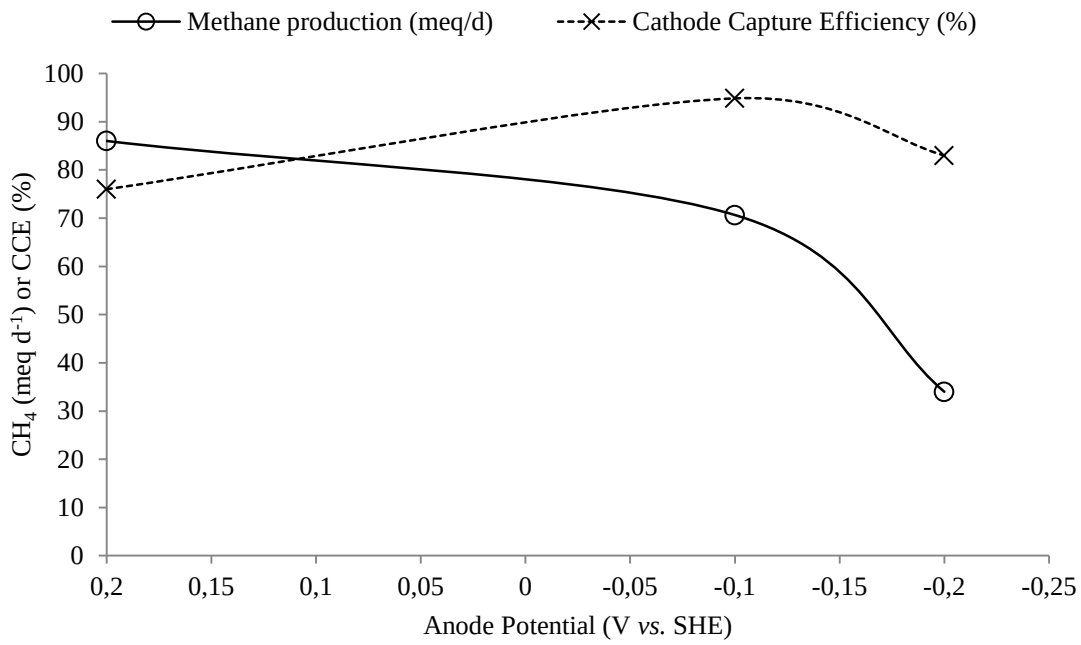


Figure 5.2 - Performance of the MEC as a function of the set anode potential in terms of average methane production rate and cathode capture efficiency.

The energy efficiency ($\eta_E$) of the MEC refers to the energy that is captured into methane gas relative to the electrical input. For an applied potential of +0.2 V *vs.* SHE it is obtained 71 % of this efficiency (Figure 5.3), which indicates that energy recovery is less than energy input. In contrast, at more negative anodic potentials a substantial energy recovery of the system is observed, that actually overcome 100% (specifically 137.17 % and 152 % for -0.1 and -0.2 V, respectively). This increase is due to the important role the potential difference, established between the cathode and the anode' system, takes in the calculation of this parameter (see Equation 3.35 and 3.36). In fact a decrease in the $\Delta V$ was observed with the decrease at the set anode potential, specifically at -0.2 V the $\Delta V$ of the system accounted for -0.58 ± 0.02 V, and at -0.1 V the $\Delta V$ increased to -0.74 ± 0.01 V, which consequently led to higher energy efficiency at -0.2 V *vs.* SHE.

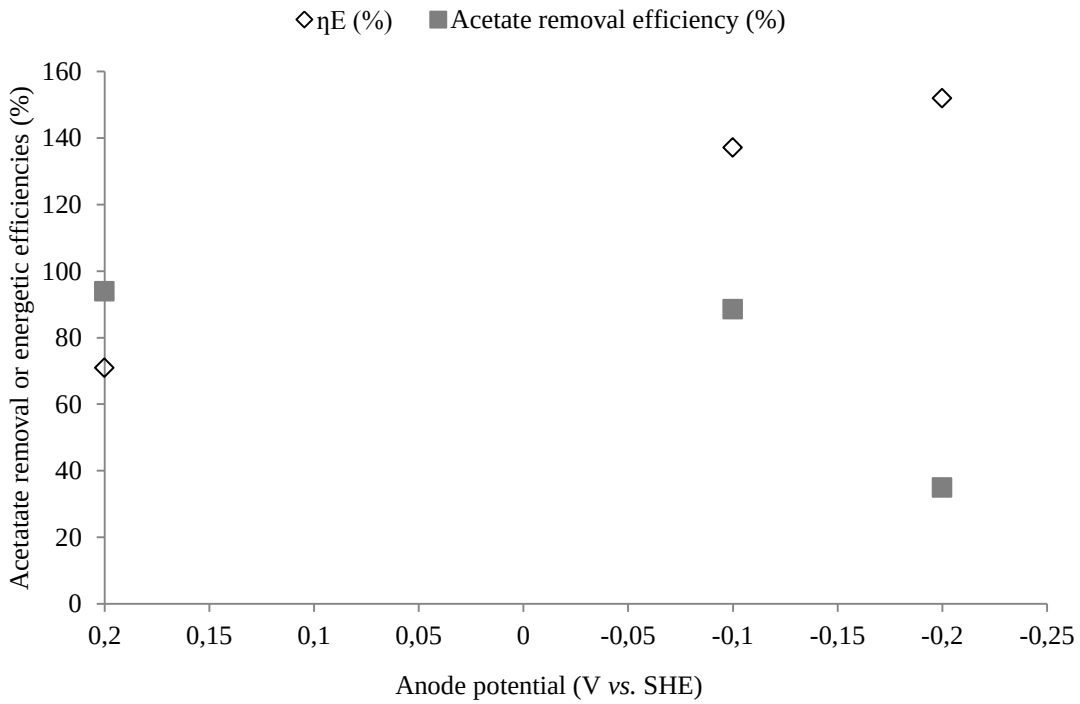


Figure 5.3 - Performance of the MEC as a function of the set anode potential in terms of energy efficiency and acetate removal efficiency.

The overall remark of the reactor performance at different applied potentials is that controlling the anode potential at -0.1 V it is simultaneously observed high energy efficiency and significant acetate removal, indicating that this is the best operating condition between those investigated.

## 5.2. Effect of different substrates on MEC performance

As earlier described, this research also studied the reactor's performance while being fed with two different substrates: a solution containing acetate as sole carbon source in Run I, and a more complex solution containing organic compounds other than acetate in Run II. Likewise the MEC performance in both conditions is compared in this paragraph.

In the previous paragraph the first period of Run I operation (when the reactor had the highest performance) was used to investigate the effect of the anode potential. However, as explained in the Results chapter, the performance of the reactor decreased throughout the experimentation, which was also confirmed with the hydrodynamic characterization of the bioanode. Therefore the last period of Run I, which goes from day 74 until day 85 will be compared with Run II, since this two periods are the timeliest close.

In Figure 5.4 an overview of the bioanode performance with both substrates is presented. As discussed in the Results chapter, the current output immediately decreases when the feeding solution was switched from acetate to the more complex solution, attaining an average value of 27.13 mA against previous 43.68 mA. In spite of low current output for the Run I (last period), the acetate removal was still high; thus, the CE for this condition was low (compared to the previous performance). Regarding Run II results, the total COD removal was around 63 %, yet individual acetate consumption, of 84 %, was identical to Run I performance. Since the percentage of acetate in the complex synthetic solution was 10.7 %, the MEC achieved a COD removal (different from acetate) over 50 %. Here the results are interesting as the CE for the synthetic wastewater feed is higher than the one of the acetate feed. This was not expected since the synthetic wastewater contains fermentable substrates implying its consumption by diverse competing metabolisms. Another remarkable result is the calculation of the CE considering only acetate, which arises to 216.11%. This result is impossible, as CE cannot exceed 100%, in this manner it is possible to state that the produced current resulted from degradation of compounds present in the synthetic wastewater, others than acetate.

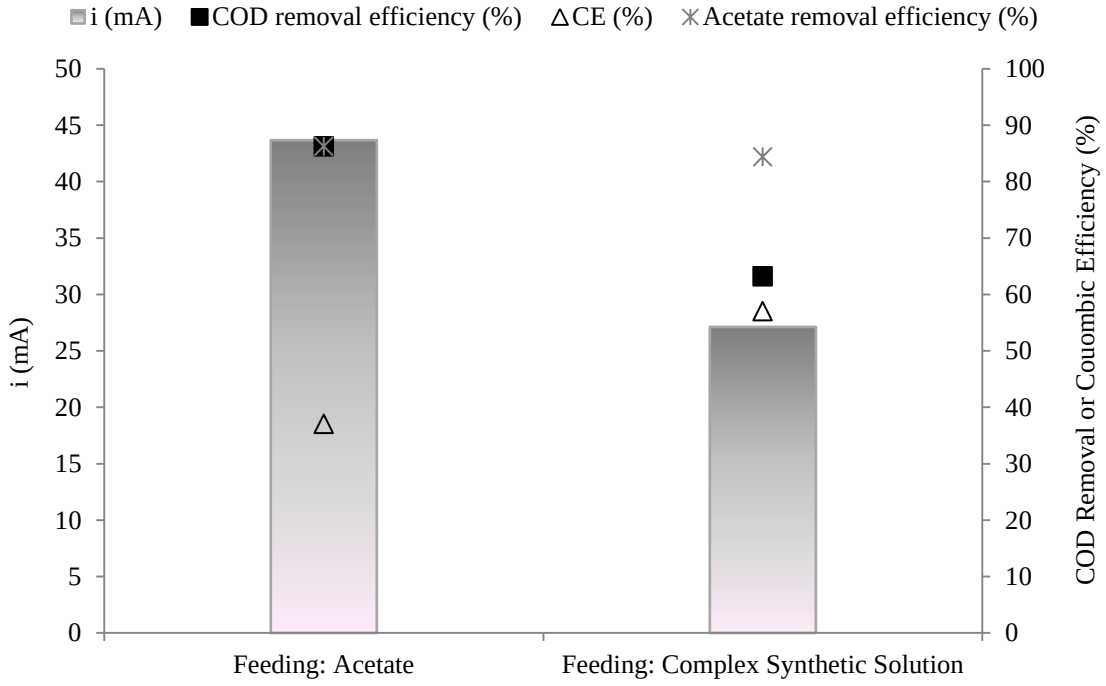


Figure 5.4 - Performance of the MEC anode with respect to the type of substrate.

Concerning methane production rate, it sharply decreases from 43.06 to 15.01 meq $d^{-1}$ when the substrate is changed, as seen in Figure 5.5. On the other hand, the CCE average value is 90 % for the complex synthetic substrate, far from the 135 % of the period being compared. Nevertheless, assuming that all the removed acetate from substrate is diverted into methane it

was expected a production rate around 9 meq $d^{-1}$. As the obtained rate is more than 50 % higher, it suggests that produced methane was originated from electrons coming from COD other than acetate.

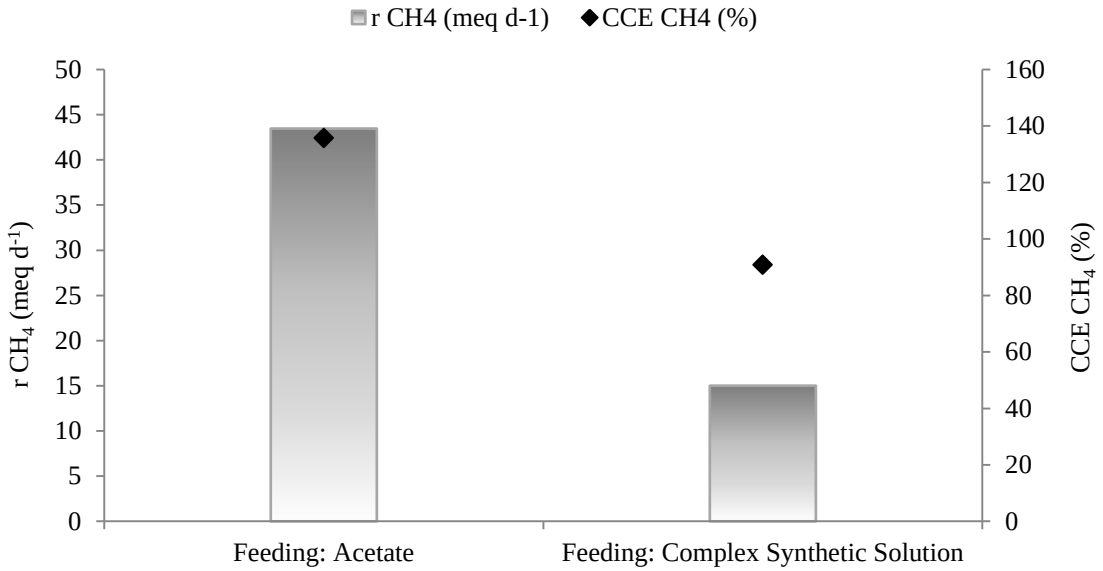


Figure 5.5 - Performance of the MEC with respect to substrate type in terms of average methane production rate and cathode capture efficiency.

Regarding the energy efficiency, a net positive energy recovery is observed with both substrates, accounting for 217.71 % and 169.76 % for the acetate solution and the more complex solution, respectively.

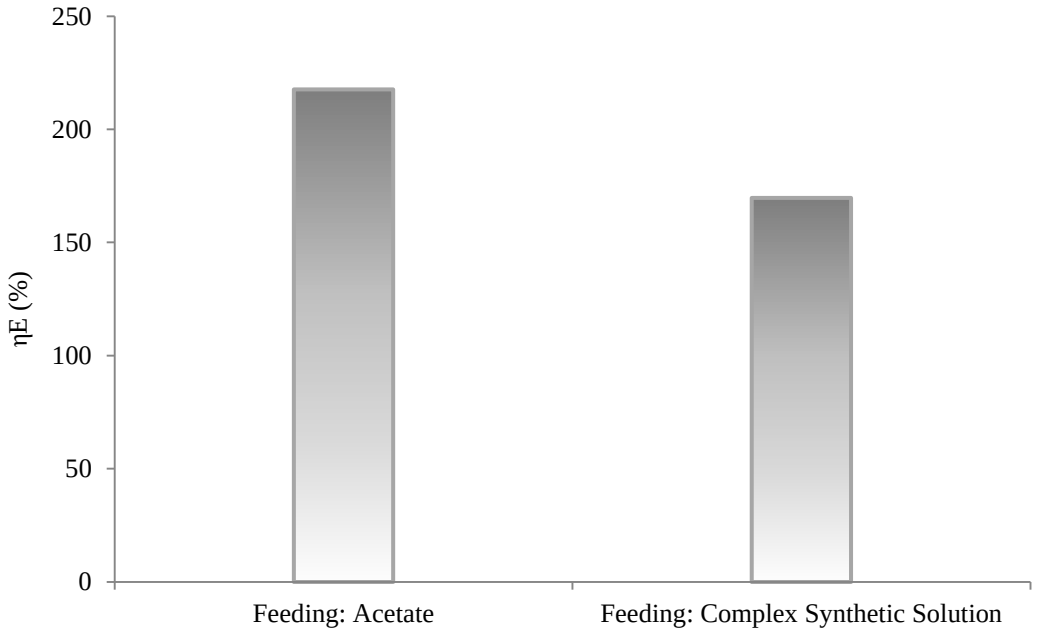


Figure 5.6 - Performance of the MEC with respect to substrate type in terms of energy efficiency and acetate removal efficiency.

### 5.3. Fluid dynamics of the MEC

As previously described, the reactor performance decreased throughout the experimentation. Accordingly, the purpose of this section is to explain the reasons through the hydrodynamic characterization of the MEC.

In chapter 4.2 Hydrodynamic characterization of the bioanode, the results of two tracer experiments have been described. Besides these two, a first tracer experiment had been previously carried out, as described in Villano, Aulenta, Beccari, et al. 2012. The main results for the three experiments are presented in Table 5.1. Figure 5.8 shows the three tracer experiments with the respective F(t) curves. As it is observed, in the first trial (referred to as October 2011) the bioanode hydrodynamic response fits the behavior of a continuous-stirred tank reactor (CSTR). As for the second test, carried out in May, a lag phase of 2.5 h is observed, result that is also recorded in the last tracer experiment (referred to as June 2012), although with a more extended lag phase, that persisted for 4 h. These results indicate a change in the MEC fluid dynamics, which was likely linked to the decrease of the produced current. As described in Results chapter, at the time of second tracer experiment the reactor was no longer working as a CSTR, and the proposed model for the reactor fluid dynamics was the combination of a PFR and a CSTR with a stagnant space, pointing in this difference a possible cause to the current's output decline observed before the second tracer experiment. Actually, in a certain time of the experimental work, a collapse of the graphite bed was visible in the reactor (Figure 5.7); this

empty space may be equivalent to the stagnant zone proposed in the theoretical model. Also the lack of graphite in the reactor represents an absence of support to microorganisms, which could suggest the declining in microbial activity and consequently the less current generation.

Figure 5.7 - Visible lack of graphite in the reactor chamber.

As for the calculated hydraulic retention time HRT, it accounted for 11.1 h in the second tracer experiment, which represents an increase of 33.5 % from the first experiment (7.38 h), that suggests an increase of empty volume in the reactor (i.e. due to graphite collapse), that was likely combined with a progressive and slow negative drift of the feed flow rate. In this manner the organic volumetric load rate that was being fed to the system was also affected, getting lower, which consequently causes a decrease in the current output. The last trial was performed after Run II, and a HRT of 10.42 h was achieved, indicating a further change in the MEC performance, likely due to a change in the graphite granules configuration.

Table 5.1 - Operating conditions and main results of the three performed tracer experiments for the MEC.

| | **October 2011** | **May 2012** | **June 2012** |
|---|---|---|---|
| **HRT (h)** | 7,38 | 11,1 | 10,42 |
| $\boldsymbol{v}$ **(mL/min)** | 1 | 0,87 | 1 |
| $\mathbf{HRT_T}$ **(h)** | 14,33 | 16,48 | 14,33 |
| $\boldsymbol{\varepsilon_0}$ | 0,51 | 0,67 | 0,73 |

From another point of view, by taking into account HRT and $HRT_T$ (which was calculated by considering the total empty volume of the MEC anode) it is possible to calculate the bed porosity inside the reactor, for the three trials. The bed porosity has increased from 0.51 to 0.73, that can be due to graphite's granules degradation inside the reactor. Furthermore as previously stated in Results paragraph on 4.3 Scanning Electron Microscopy (SEM), the cavities in the used graphite seem to be wider than those in the fresh graphite, which also suggests the possible degradation of the granules. As an additional effect, the biofilm deposits on the membrane, clearly observed in the SEM images, could lead to adverse effects on the mass transport through the membrane, due to the physical barrier of the biofilm that could reduce the proton migration, leading again to less current production. Finally, it is possible that the micrometric ruptures visible in the membrane (Figure 4.17 D) caused a short circuit of the acetate, from the anode chamber to the cathode, a circumstance that could explain the decrease in the anodic coulombic efficiency and the simultaneous increase in the cathodic capture efficiency, as stated in a previous paragraph.

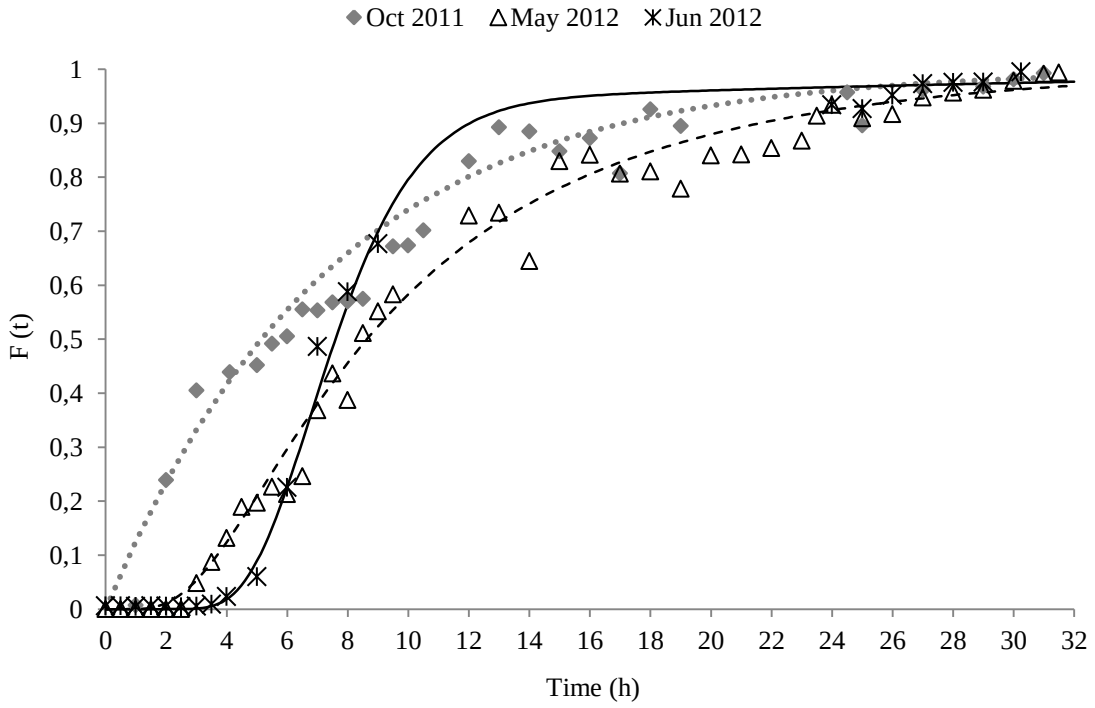


Figure 5.8 - Trend of the three tracer experiments carried out throughout the MEC operation.

# 6. Conclusive remarks and future perspectives

The results obtained in this research demonstrated the possibility to couple organic matter oxidation and biogas production, more specifically methane, in a fully biological two-chamber microbial electrolysis cell (MEC). The performance of the MEC was studied concerning different feeding solutions, at the same applied anode potential. Furthermore, the effect of the anode potential on the MEC performance was also considered, in comparison with previous experiments.

Main attention was paid to the MEC performance when continuously feeding the anode chamber with an acetate solution as substrate, at an applied organic load rate (OLR) of 1.08 gCOD $L^{-1}$ $d^{-1}$, and the anode potential controlled at -0.1 V *vs.* SHE (Run I). In these conditions the MEC presented, at its highest performance, an anodic acetate removal of 88 ± 2 %, being the resulting electron flow mainly recovered at the cathode as methane, with a production rate of 71 meq $d^{-1}$. The coulombic efficiency (CE) at the anode accounted for 73 %. While for cathode capture efficiency (CCE) accounted for 95 %; hence both anode and cathode were quite specific and efficient. Overall, the energy efficiency of the system, i.e., the amount of energy potentially captured into produced methane relative to the electrical energy input was 137 ± 6 %.

At the time of this experimentation, the MEC had been efficiently operated for more than 12 months. However, during my thesis work, a decrease in the outcomes of the reactor was observed over time. Among several hypotheses, it is worth noting that the decrease of current and CE over time occurred together with an increase of CCE. Based on the SEM images acquired from the proton exchange membrane, it presented some micrometric ruptures which possibly caused a short circuit for the acetate to be transferred from the anode to the cathode chamber, resulting in a decrease of current that was associated to an apparently high CCE.

Run II was operated by using a synthetic solution containing soluble organic compounds along with a little percentage of acetate: the current output of the reactor was lower than the value achieved with acetate as the only substrate (27.13 mA against 43.68 mA). The total COD removal was around 63 %, yet individual acetate consumption (84 %) was identical to Run I performance. On the coulombic efficiency calculation, Run II revealed interesting results. The CE was higher for the synthetic wastewater feed (57.01 % against 37.06 %) which was not expected since this substrate contains fermentable compounds implying its consumption by diverse competing metabolisms. Another remarkable result is the calculation of the CE considering only acetate (216.11 %), that confirms that the produced current also resulted from oxidation of compounds present in the synthetic wastewater, others than acetate. Concerning the biogas production, the main reaction occuring at the cathode was methane generation, with an

average rate of 17.92 meq $d^{-1}$, accounting for about 90 % of CCE. The energy efficiency of the system was 170 ± 11 %.

The evaluation of the system when submitted to different anode potentials, revealed a close correlation between current generation and acetate consumption, which clearly indicates the ability of the inoculated sludge to use the graphite anode as terminal electron acceptor for the electrochemical substrate oxidation in a large range of applied potentials. It is worth noting that also the rate of methane production at the cathode follows the trend of acetate removal; hence, the explanation for the lower methane production is due to the lower anode potential and consequently the lower current output. The energy efficiency of the MEC is higher at lower anodic potentials (specifically 137.17 % and 152 % for -0.1 and -0.2 V, respectively). This is owed to the important role the potential difference established between the cathode and the anode takes in the calculation of this parameter. The overall remark of the reactor performance at different applied potentials is that controlling the anode potential at -0.1 V *vs.* SHE it is simultaneously observed high energy efficiency and significant acetate removal, showing this is the best operating condition between those investigated.

Furthermore, very low biomass growth was observed at the anode as well as very high concentration of ammonium ion at the cathode compartment in both Run I and Run II.

The first evidence, low biomass growth, suggests that MEC could offer a valid alternative to existing processes for wastewater treatment, since it has the potential to decrease the operating cost for two key factors (i.e. the management of the produced sludge and the energy demand for oxygen supply). The obtained results show that sludge production would be very low because of the low biomass growth yields, as well as less or even no energy could be required due to the possible energy recovery from methane production.

The second evidence, high ammonium concentration at the cathode, is related to the transport of ammonium across the membrane, from the anode to the cathode. Even though not specifically optimized in this thesis, this ammonium preferential flow could offer a new perspective for ammonium removal from wastewater, as an alternative to biological nitrification (i.e. a biological reaction that has a high oxygen demand and is rather sensitive to changes of environmental conditions).

Overall, these findings suggest that a methane-producing MEC can be used for treatment of low-strength wastewater, with good energy efficiency and very low sludge production.

Moreover, this type of system could allow adding higher energetic and economical value to both the liquid and gaseous effluent from the anaerobic digestion (AD). In point of fact, the MEC anode could be effective to remove from the liquid effluent the residual volatile fatty acids and

ammonium, the latter being concentrated into the biogas compartment and recovered or removed by stripping. As regards the AD biogas, it could be upgraded at the MEC cathode by means of decreasing its carbon dioxide content and simultaneously increasing the methane content.

As future works it is proposed to verify the performance of the reactor with low-strength wastewater or effluents from sludge anaerobic digesters, and also the microbial characterization of the bioanode and biocathode through biomolecular tools.

# 7. Bibliography


Agler, M.T. et al., 2011. Waste to bioproduct conversion with undefined mixed cultures: the carboxylate platform. *Trends in biotechnology*, 29(2), pp.70–8. Available at: http://www.ncbi.nlm.nih.gov/pubmed/21190748.

Angenent, L.T. et al., 2004. Production of bioenergy and biochemicals from industrial and agricultural wastewater. *Trends in biotechnology*, 22(9), pp.477–85. Available at: http://www.ncbi.nlm.nih.gov/pubmed/15331229.

APHA, 1995. *Standard Methods for the Examination of Water and Wastewater.*, Washingtons, DC.

Appleby, A.J. & Yeager, E.B., 1986. Solid Polymer Electrolyte Fuel Cells (SPEFCs). *Energy*, 11(1-2), pp.137–152.

Aulenta, F. et al., 2007. Electron transfer from a solid-state electrode assisted by methyl viologen sustains efficient microbial reductive dechlorination of TCE. *Environmental science & technology*, 41(7), pp.2554–9. Available at: http://www.ncbi.nlm.nih.gov/pubmed/17438815.

Aulenta, F. et al., 2009. Microbial reductive dechlorination of trichloroethene to ethene with electrodes serving as electron donors without the external addition of redox mediators. *Biotechnology and bioengineering*, 103(1), pp.85–91. Available at: http://www.ncbi.nlm.nih.gov/pubmed/19160378.

Aulenta, F. et al., 2010. The humic acid analogue antraquinone-2,6-disulfonate (AQDS) serves as an electron shuttle in the electricity-driven microbial dechlorination of trichloroethene to cis-dichloroethene. *Bioresource technology*, 101(24), pp.9728–33. Available at: http://www.ncbi.nlm.nih.gov/pubmed/20709536.

Aulenta, F. et al., 2011. Dechlorination of trichloroethene in a continuous-flow bioelectrochemical reactor: effect of cathode potential on rate, selectivity, and electron transfer mechanisms. *Environmental science & technology*, 45(19), pp.8444–51. Available at: http://www.ncbi.nlm.nih.gov/pubmed/21877695.

Balch, W.E. et al., 1979. Methanogens: reevaluation of a unique biological group. *Microbiological reviews*, 43(2), pp.260–96. Available at: http://www.pubmedcentral.nih.gov/articlerender.fcgi?artid=281474&tool=pmcentrez&rendertype=abstract.

Bond, D.R. & Lovley, D.R., 2003. Electricity Production by Geobacter sulfurreducens Attached to Electrodes. *Applied and Environmental Microbiology*, 69(3), pp.1548–1555.

Call, D.F., Merrill, Matthew D. & Logan, B.E., 2009. High surface area stainless steel brushes as cathodes in microbial electrolysis cells. *Environmental science & technology*, 43(6), pp.2179–83. Available at: http://www.ncbi.nlm.nih.gov/pubmed/19368232.

Von Canstein, H. et al., 2008. Secretion of flavins by Shewanella species and their role in extracellular electron transfer. *Applied and environmental microbiology*, 74(3), pp.615–23. Available at: http://aem.asm.org/cgi/content/long/74/3/615.

Chae, K.-J. et al., 2008. Mass Transport through a Proton Exchange Membrane ( Nafion ) in Microbial Fuel Cells †. *Energy & Fuels*, 22(1), pp.169–176.

Cheng, S., Liu, H. & Logan, B.E., 2006. Power densities using different cathode catalysts (Pt and CoTMPP) and polymer binders (nafion and PTFE) in single chamber microbial fuel cells. *Environmental science & technology*, 40(1), pp.364–9. Available at: http://www.ncbi.nlm.nih.gov/pubmed/16433373.

Cheng, S. et al., 2009. Direct biological conversion of electrical current into methane by electromethanogenesis. *Environmental science & technology*, 43(10), pp.3953–8. Available at: http://www.ncbi.nlm.nih.gov/pubmed/19544913.

Clauwaert, P., Rabaey, K., et al., 2007. Biological denitrification in microbial fuel cells. *Environmental science & technology*, 41(9), pp.3354–60. Available at: http://www.ncbi.nlm.nih.gov/pubmed/17539549.

Clauwaert, P., Van der Ha, D., et al., 2007. Open air biocathode enables effective electricity generation with microbial fuel cells. *Environmental science & technology*, 41(21), pp.7564–9. Available at: http://www.ncbi.nlm.nih.gov/pubmed/18044542.

Cord-Ruwisch, R., Law, Y. & Cheng, K.Y., 2011. Ammonium as a sustainable proton shuttle in bioelectrochemical systems. *Bioresource technology*, 102(20), pp.9691–6. Available at: http://www.ncbi.nlm.nih.gov/pubmed/21865037.

Du, Z., Li, H. & Gu, T., 2007. A state of the art review on microbial fuel cells : A promising technology for wastewater treatment and bioenergy. *Biotechnology Advances*, 25, pp.464–482.

Foley, J.M. et al., 2010. Life Cycle Assessment of High-Rate Anaerobic Treatment, Microbial Fuel Cells, and Microbial Electrolysis. *Environmental science & technology*, 44(9), pp.3629–3637.

Freguia, S., Rabaey, K. & Yuan, Z., 2007. Non-catalyzed cathodic oxygen reduction at graphite granules in microbial fuel cells. *Electrochimica Acta*, 53(2), pp.598–603.

Goldemberg, J. & Johansson, T.B., 2004. *World Energy Assessment Overview: 2004 Update*, New York: United Nations Development Programme.

Gregory, K.B., Bond, D.R. & Lovley, D.R., 2004. Graphite electrodes as electron donors for anaerobic respiration. *Environmental microbiology*, 6(6), pp.596–604. Available at: http://www.ncbi.nlm.nih.gov/pubmed/15142248.

Harnisch, F. & Schröder, U., 2010. From MFC to MXC: chemical and biological cathodes and their potential for microbial bioelectrochemical systems. *Chemical*

*Society reviews*, 39(11), pp.4433–48. Available at: http://www.ncbi.nlm.nih.gov/pubmed/20830322.

Heilmann, J. & Logan, B.E., 2006. Production of Electricity from Proteins Using a Microbial Fuel Cell. *Water Environment Research*, 78(5), pp.531–537. Available at: http://www.ingentaselect.com/rpsv/cgi-bin/cgi?ini=xref&body=linker&reqdoi=10.2175/106143005X73046.

IEA, 2010. *World Energy Outlook 2010*, International Energy Agency.

Jacobson, K.S., Drew, D.M. & He, Z., 2011. Efficient salt removal in a continuously operated upflow microbial desalination cell with an air cathode. *Bioresource technology*, 102(1), pp.376–80. Available at: http://www.ncbi.nlm.nih.gov/pubmed/20584603.

Kiely, P.D., Regan, J.M. & Logan, B.E., 2011. The electric picnic: synergistic requirements for exoelectrogenic microbial communities. *Current opinion in biotechnology*, 22(3), pp.378–85. Available at: http://www.ncbi.nlm.nih.gov/pubmed/21441020.

Kim, H.J. et al., 2002. A mediator-less microbial fuel cell using a metal reducing bacterium, Shewanella putrefaciens. *Enzyme and Microbial Technology*, 30(2), pp.145–152. Available at: http://linkinghub.elsevier.com/retrieve/pii/S0141022901004781.

Kim, J.R. et al., 2007. Electricity generation and microbial community analysis of alcohol powered microbial fuel cells. *Bioresource technology*, 98(13), pp.2568–77. Available at: http://www.ncbi.nlm.nih.gov/pubmed/17097875.

Kleerebezem, R. & Van Loosdrecht, M.C.M., 2007. Mixed culture biotechnology for bioenergy production. *Current opinion in biotechnology*, 18(3), pp.207–12. Available at: http://www.ncbi.nlm.nih.gov/pubmed/17509864.

Kuntke, P. et al., 2011. Effects of ammonium concentration and charge exchange on ammonium recovery from high strength wastewater using a microbial fuel cell. *Bioresource technology*, 102(6), pp.4376–82. Available at: http://www.ncbi.nlm.nih.gov/pubmed/21277769.

Liu, H., Ramnarayanan, R. & Logan, B.E., 2004. Production of electricity during wastewater treatment using a single chamber microbial fuel cell. *Environmental science & technology*, 38(7), pp.2281–5. Available at: http://www.ncbi.nlm.nih.gov/pubmed/20889062.

Liu, H., Cheng, S. & Logan, B.E., 2005. Production of electricity from acetate or butyrate using a single-chamber microbial fuel cell. *Environmental science & technology*, 39(2), pp.658–62. Available at: http://www.ncbi.nlm.nih.gov/pubmed/15707069.

Liu, H., Grot, S. & Logan, B.E., 2005. Electrochemically assisted microbial production of hydrogen from acetate. *Environmental science & technology*, 39(11), pp.4317–20. Available at: http://www.ncbi.nlm.nih.gov/pubmed/15984815.

Logan, B.E. et al., 2005. Electricity generation from cysteine in a microbial fuel cell. *Water research*, 39(5), pp.942–52. Available at: http://www.ncbi.nlm.nih.gov/pubmed/15743641.

Logan, B.E. et al., 2006. Microbial Fuel Cells : Methodology and Technology. *Environmental Science & Technology*, 40(17), pp.5181–5192.

Logan, B.E., 2009. Exoelectrogenic bacteria that power microbial fuel cells. *Nature reviews. Microbiology*, 7(5), pp.375–81. Available at: http://www.ncbi.nlm.nih.gov/pubmed/20632002.

Lovley, D.R., 2008. Extracellular electron transfer: wires, capacitors, iron lungs, and more. *Geobiology*, 6(3), pp.225–31. Available at: http://www.ncbi.nlm.nih.gov/pubmed/18393985.

Mauritz, K.A. & Moore, R.B., 2004. State of understanding of nafion. *Chemical reviews*, 104(10), pp.4535–85. Available at: http://www.ncbi.nlm.nih.gov/pubmed/15669162.

Mehanna, M. et al., 2010. Microbial electrodialysis cell for simultaneous water desalination and hydrogen gas production. *Environmental science & technology*, 44(24), pp.9578–83. Available at: http://www.ncbi.nlm.nih.gov/pubmed/21077623.

Min, B. & Logan, B.E., 2004. Continuous electricity generation from domestic wastewater and organic substrates in a flat plate microbial fuel cell. *Environmental science & technology*, 38(21), pp.5809–14. Available at: http://www.ncbi.nlm.nih.gov/pubmed/15575304.

Min, B. et al., 2005. Electricity generation from swine wastewater using microbial fuel cells. *Water research*, 39(20), pp.4961–8. Available at: http://www.ncbi.nlm.nih.gov/pubmed/16293279.

Pant, D. et al., 2010. A review of the substrates used in microbial fuel cells (MFCs) for sustainable energy production. *Bioresource technology*, 101(6), pp.1533–43. Available at: http://www.ncbi.nlm.nih.gov/pubmed/19892549.

Pant, D. et al., 2011. An introduction to the life cycle assessment (LCA) of bioelectrochemical systems (BES) for sustainable energy and product generation: Relevance and key aspects. *Renewable and Sustainable Energy Reviews*, 15(2), pp.1305–1313. Available at: http://linkinghub.elsevier.com/retrieve/pii/S136403211000345X.

Pham, T.H. et al., 2006. Microbial Fuel Cells in Relation to Conventional Anaerobic Digestion Technology. *Engineering in Life Sciences*, 6(3), pp.285–292. Available at: http://doi.wiley.com/10.1002/elsc.200620121.

Rabaey, K. et al., 2005. Microbial phenazine production enhances electron transfer in biofuel cells. *Environmental science & technology*, 39(9), pp.3401–8. Available at: http://www.ncbi.nlm.nih.gov/pubmed/15926596.

Rabaey, K. & Verstraete, W., 2005. Microbial fuel cells: novel biotechnology for energy generation. *Trends in biotechnology*, 23(6), pp.291–8. Available at: http://www.ncbi.nlm.nih.gov/pubmed/15922081.

Rabaey, K. et al., 2010. High current generation coupled to caustic production using a lamellar bioelectrochemical system. *Environmental science & technology*, 44(11), pp.4315–21. Available at: http://www.ncbi.nlm.nih.gov/pubmed/20446659.

Rabaey, K. & Rozendal, R.A., 2010. Microbial electrosynthesis - revisiting the electrical route for microbial production. *Nature reviews. Microbiology*, 8(10), pp.706–16. Available at: http://www.ncbi.nlm.nih.gov/pubmed/20844557.

Reguera, G. et al., 2005. Extracellular electron transfer via microbial nanowires. *Nature*, 435, pp.1098–1101.

Rosenbaum, M., He, Z. & Angenent, L.T., 2010. Light energy to bioelectricity: photosynthetic microbial fuel cells. *Current opinion in biotechnology*, 21(3), pp.259–64. Available at: http://www.ncbi.nlm.nih.gov/pubmed/20378333.

Rozendal, R.A., 2006. Effects of Membrane Cation Transport on pH and Microbial Fuel Cell Performance. *Environmental Science & Technology*, 40(17), pp.5206–5211.

Rozendal, R.A. et al., 2006. Principle and perspectives of hydrogen production through biocatalyzed electrolysis. *International Journal of Hydrogen Energy*, 31(12), pp.1632–1640. Available at: http://linkinghub.elsevier.com/retrieve/pii/S0360319905003903.

Rozendal, R.A. et al., 2008. Hydrogen Production with a Microbial Biocathode. *Environmental Science & Technology*, 42(2), pp.629–634. Available at: http://pubs.acs.org/doi/abs/10.1021/es071720+.

Schiermeier, Q. et al., 2008. Energy alternatives: Electricity without carbon. *Nature*, 454(August), pp.816–823.

Selembo, P.A., Merrill, Mathew D. & Logan, B.E., 2009. The use of stainless steel and nickel alloys as low-cost cathodes in microbial electrolysis cells. *Journal of Power Sources*, 190(2), pp.271–278. Available at: http://linkinghub.elsevier.com/retrieve/pii/S037877530900038X.

Sleutels, T.H.J.A. et al., 2009. Improved performance of porous bio-anodes in microbial electrolysis cells by enhancing mass and charge transport. *International Journal of Hydrogen Energy*, 34(24), pp.9655–9661. Available at: http://linkinghub.elsevier.com/retrieve/pii/S0360319909015298.

Sleutels, T.H.J.A., Hamelers, H.V.M. & Buisman, C.J.N., 2011. Effect of mass and charge transport speed and direction in porous anodes on microbial electrolysis cell

performance. *Bioresource technology*, 102(1), pp.399–403. Available at: http://www.ncbi.nlm.nih.gov/pubmed/20619642.

Venkataraman, A. et al., 2010. Quorum sensing regulates electric current generation of Pseudomonas aeruginosa PA14 in bioelectrochemical systems. *Electrochemistry Communications*, 12(3), pp.459–462. Available at: http://linkinghub.elsevier.com/retrieve/pii/S1388248110000305.

Villano, M. et al., 2010. Bioelectrochemical reduction of CO(2) to CH(4) via direct and indirect extracellular electron transfer by a hydrogenophilic methanogenic culture. *Bioresource technology*, 101(9), pp.3085–90. Available at: http://www.ncbi.nlm.nih.gov/pubmed/20074943.

Villano, M. et al., 2011. Electrochemically assisted methane production in a biofilm reactor. *Journal of Power Sources*, 196(22), pp.9467–9472. Available at: http://linkinghub.elsevier.com/retrieve/pii/S0378775311013541.

Villano, M., Aulenta, F., Beccari, M., et al., 2012. Start-up and Performance of an Activated Sludge Bioanode in Microbial Electrolysis Cells. *Chemical Engineering Transactions*, 27, pp.109–114.

Villano, M., Aulenta, F. & Majone, M., 2012. Perspectives of biofuels production from renewable resources with bioelectrochemical systems. *Asia-Pacific Journal of Chemical Engineering*, 7(S3), pp.S236–S274.

Villano, M. et al., 2013. Carbon and nitrogen removal and enhanced methane production in a microbial electrolysis cell. *Bioresource technology*, 130, pp.366–371. Available at: http://www.ncbi.nlm.nih.gov/pubmed/23313682.

Wall, J.D., Harwood, C.S. & Demain, A., 2008. *Bioenergy*, Washingtons, DC: ASM Press.

Wei, J. et al., 2010. A New Insight into Potential Regulation on Growth and Power Generation of Geobacter sulfurreducens in Microbial Fuel Cells Based on Energy Viewpoint. , 44(8), pp.3187–3191.

Zeikus, J.G., 1977. The Biology of Methanogenic Bacteria. *Bacteriological Reviews*, 41(2), pp.514–541.

Zeng, K. & Zhang, D., 2010. Recent progress in alkaline water electrolysis for hydrogen production and applications. *Progress in Energy and Combustion Science*, 36(3), pp.307–326. Available at: http://dx.doi.org/10.1016/j.pecs.2009.11.002.

Zhao, F. et al., 2005. Application of pyrolysed iron(II) phthalocyanine and CoTMPP based oxygen reduction catalysts as cathode materials in microbial fuel cells. *Electrochemistry Communications*, 7(12), pp.1405–1410. Available at: http://linkinghub.elsevier.com/retrieve/pii/S1388248105002912.